ESTIMATING CAPACITY OF OFFSHORE FOUNDATIONS

J.D. Murff, Ph.D. P.E., Dist. M. ASCE

Consultant, Austin, Texas USA
Formerly Visiting Professor, Texas A&M Univ., College Station, Texas, USA
Formerly Sr. Research Advisor, Exxon Production Research Co., Houston, Texas, USA

Abstract
This paper will describe a range of techniques for estimating the capacity of offshore foundations which has always been a main issue in foundation design and remains so today. In so doing the paper will, however, take a tack that is slightly out of the mainstream - emphasizing methods of plastic limit analysis rather than more traditional approaches. It begins with a brief history of offshore geotechnical developments describing how design methods have evolved for shallow foundations and pile foundations and emphasizing the types of loads, site conditions, and foundation geometries encountered. A number of simple solutions are provided with detailed example problems. It is the author's view that plastic limit analysis methods have the potential to supplement and enhance more traditional methods.

1. Introduction

I am sincerely honoured to be invited to give the inaugural McClelland Lecture. I am humbled by the task before me as I sincerely wish to produce something that Bram McClelland would have appreciated. At first I leaned toward a subject that more characterised his expertise and interest- engineering geology, site investigation, and foundation design. On further reflection however I concluded that Bram delighted in developing engineers who followed their own interests, not in his image, but in their own unique ways. That is the kind of leader he was. This epiphany led me to select a topic that has long been a passion of mine - bridging the gap, sometimes chasm, between theory and practice. I believe this is what he would have wanted from me.

Estimating foundation capacity has always been a central issue in foundation analysis and design. Many different methods are employed in this practice and many of those involve ad hoc assumptions and empirical models. While these methods have served the profession well, advancements have been made that have not always been fully exploited. In this paper we will focus on one such advancement, plastic limit analysis (PLA), a methodology that is theoretically sound, internally consistent, and surprisingly simple to apply. In my experience I have found this approach can lend significant advantages to some of the more traditional methods. The fact that PLA is underutilized by practicing engineers stems partly, I think, from a literature that tends to be heavily mathematical and often arcane. The main purpose of the paper then is to take a small step towards demystifying the concepts for the mainstream using a number of detailed examples. The examples are intentionally simple ones so that detailed results can be presented without getting too bogged down in the theory.

Many of the problems encountered in offshore foundation engineering are particularly well suited for applying PLA methods. We will first provide a general overview of foundation types that are used in the offshore environment. This will be in an historical context working the way from early offshore beginnings such as piers and jackets to modern issues of deep water applications. In the illustrations of the analysis techniques involved we will define a limited number of idealised foundations along with typical loading scenarios. We will then demonstrate how capacity estimates can be made using a range of available solutions in the framework of PLA. Typical cases will be analysed including shallow foundations, pile foundations, and systems of these types. In the process we will put special emphasis on characterising results using multi-axial failure interaction diagrams. Finally we will discuss the similarities and differences in PLA methods and more traditional limit equilibrium approaches.

2. A Brief History

Offshore drilling was initially carried out from piers extending from the shore as early as the late 1800's as shown in Figure 1. Over the next 50 years, "offshore drilling" was done from a wide variety of platforms including barges, piled platforms, and dredged islands. These platforms were sited in the shallow bays, marshes, canals etc in coastal areas such as the Gulf Coast, California Coast, Lake Maracaibo, and the Caspian Sea among others.

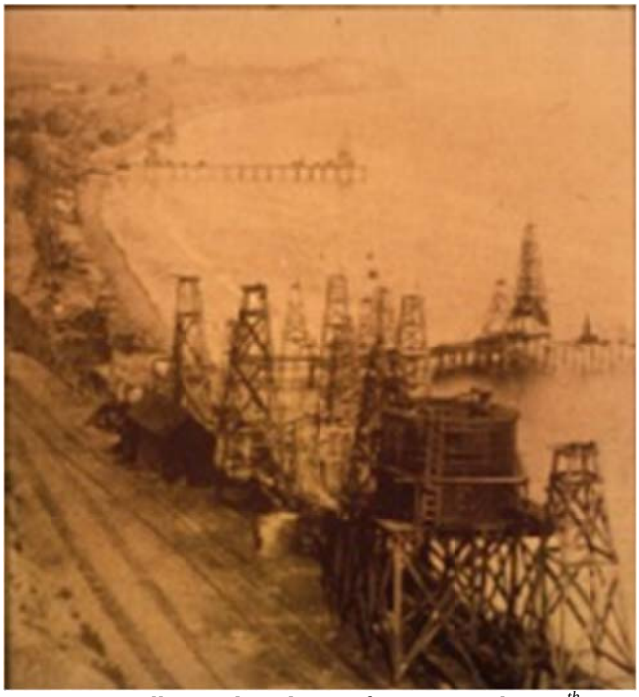

Figure 1: Drilling and production from piers in late 19th century

The first fixed offshore structure out of the sight of land, shown in Figure 2, was installed 10½ miles from the Louisiana shore in 1947 by Brown and Root for the Kerr-McGee Corporation. The following is a summary of a description in the book, "Offshore Pioneers" (Pratt, et al, 1997). The drilling deck was 38 feet by 58 feet, barely large enough for the drilling derrick. The platform was tended by a large supply barge 260 feet long. The mooring system for the barge consisted of 19 wooden pilings or dolphins arranged to buffer the platform from the barge. The platform was founded on 16, 24-inch steel pipe piles driven into the seabed 104 feet. The structure itself was vertically sided and resembled scaffolding with the piles braced with 9-3/4 inch pipe to a point two feet above mean low tide. Presumably the structure had mudmats to provide temporary support prior to pile installation. Whether there was any account taken of the lateral loads is unknown but the overturning loads were relatively small owing to the approximately 18 foot water depth. It is unlikely that there was any knowledge of the soil properties and the axial pile capacity was probably based on pile driving formulae such as the Engineering News Method (Teng, 1962) which was common practice at the time. The installation of this drilling system marked the birth of the modern offshore industry.

Figure 2: Kerr McGee installed the first offshore platform out of the sight of land

The installation of the Kerr-McGee structure was followed in rapid succession by construction of a number of other structures. Platform evolution took two distinct paths: fixed platforms for production and temporary platforms for exploration drilling. The jack-up or self-elevating platform, shown in Figure 3(a), and the floating system, shown in Figure 3(b) became the favoured concepts for exploration drilling structures but other types such as submersibles and posted barges, especially for very shallow water, have also been employed. We will not discuss these concepts further but concentrate on the foundations for permanent production platforms.

(a) *(b)*

Figure 3: Exploration drilling (a) jack-ups operate in water depths of approximately 100 m or less (b) floating vessels operate in deep water

The prefabricated, pile founded template structure, termed steel, piled jacket or SPJ, soon emerged as the structure of choice for permanent production fa-

cilities. These structures have bases larger than the decks, that is, the sides were sloped or battered to provide improved resistance to lateral loads and overturning moments. The concept evolved to address various fabrication, installation, and structural performance issues that were encountered. A schematic of a typical structure is shown in Figure 4(a) with an actual structure shown in Figure 4(b). Note the two types of piles. Main piles are inserted in and welded to the jacket legs and skirt piles are inserted and grouted into sleeves attached near the base of the structure. This configuration distributes the overturning loads relatively evenly and adds some redundancy to the overall foundation capacity. Because of the very soft soils that occur where most of these structures are placed, these jackets also have shallow foundations called mud mats that are used for temporary support before and during the pile's installation. This basic structural/foundation concept albeit with significant improvements and site modifications has remained the primary production platform for "shallow water" up to the present.

(a) *(b)*

Figure 4: Fixed bottom structures (a) schematic (b) shallow water platform

SPJs have been employed in a wide range of water depths and load environments, such as waves, currents, ice and earthquakes. The tallest platform of this type is Shell's Bullwinkle structure at 526 metres tall (1,725 feet) in a water depth of 412 metres (1,350 feet). Water depths in this range are considered about the practical limit for SPJ-type platforms. The fundamental natural period becomes such that the dynamic response under wave loading is a limiting condition and it becomes more cost effective to use floating structures with very long natural periods.

The major discoveries in the North Sea, starting in the late 1960s, posed some different challenges to the offshore industry from those in the Gulf of Mexico. The huge fields, severe winter storms and the hard, flat bottom conditions were often addressed with a new structure type, the concrete, gravity base structure or GBS, as shown in Figure 5. The GBS was found to have significant advantages over conventional platforms. These structures have large diameter, single piece bases, sometimes 100 metres or more with shear skirts that penetrate the seabed and provide lateral resistance to waves of 100 feet or more. The foundation is essentially a shallow foundation but the complex multi-axial loading environment and non-homogeneous soil conditions present a challenge not only for site investigations and interpretations but for foundation capacity analysis as well.

Figure 5: Concrete gravity structures are widely used in the central north sea

Major discoveries in very deep water such as the Gulf of Mexico, the east coast of South America, and the west coast of Africa have presented still new challenges for the marine geotechnical engineer. In these areas floating systems are primarily used to develop the resources and mooring of these systems becomes a major focus. There are a number of floating system types and many variations on each type. The anchors for the mooring systems include a range of concepts including piles, drag embedment and vertically loaded anchors, and suction caissons.

The tension leg platform with vertical tethers or tendons is usually anchored with piles to resist tension or uplift loading as shown in Figure 6(a). A few of these structures have been anchored with large gravity bases which typically use ballast to resist significant parts of the uplift load, for example the sustained uplift, whereas inverse bearing capacity and skirt friction may be designed to resist the peak environmental loads.

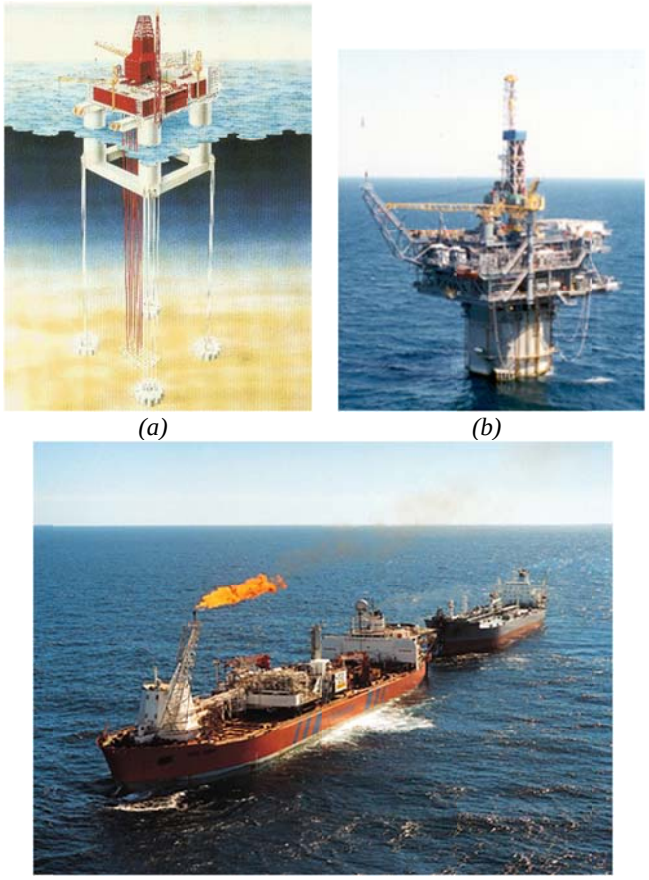

(a) *(b)*

(c)

Figure 6: Deep water production systems (a) tension leg platform (b) SPAR system (c) floating production system

Among the other floating structure types are the SPAR shown in Figure 6(b) and the floating production system or FPS shown in Figure 6(c). These structures have mooring lines that are anchored as discussed above. In addition to these concepts there are a range of submerged, bottom founded facilities deployed in deep water including manifolds, bases for steel catenary risers, subsea production systems, pipelines and pipeline end terminals (PLETs) to name a few. These structures are generally subjected to multi-axial loads and are often supported by shallow foundations or mud mats although suction caissons are also used. Another approach to support such facilities is to augment mud mats with short relatively rigid, pin piles set in the mat's corners. This added resistance can help to reduce the necessary mat dimensions which can save on installation costs. The number of different applications for mat and mat-pile foundations seems to be growing rapidly to include foundations on which to temporarily park various tools and hardware used in development.

In this paper we will consider several of the foundation concepts discussed above. We will idealise the foundation and typical load conditions and demonstrate methods for estimating ultimate capacities. As such, a brief mention of the concept of idealisation seems in order. In his excellent book, Engineering Plasticity (1969), C.R. Calladine had this to say:

"…how can mathematics, which is so clear and precise, and in so many ways simple, be applied to the physical world which, although apparently consistent, is many sided and extremely complex? The key to the solution of this problem lies in the making of idealisations of the physical world. Now we are all familiar with the process of making idealisations, but we may indeed be so familiar with it that we almost lose sight of the fact that we are making idealisations at all."

It is important to keep in mind the underlying idealisations involved when we carry out our calculations. Given that we must idealise our problems then, how do we use the results to predict behaviour or carry out designs. In this regard I am reminded of a quote (the source of which has unfortunately been lost) that my first manager cited early in my career - a quote that I have always kept in my tool kit.

" the purpose of computing is insight, not numbers"

Although we are probably all guilty of getting bogged down in the numbers from time to time, it is insight that we are trying to achieve in our calculations. How sensitive are our solutions to things we do not know so well? How likely are we to err in characterising the input to our models? How well do our idealisations represent reality? What are the consequences of performance of our foundations outside expected bounds?

While our attempt will be to illustrate general approaches to solving a range of foundation problems, we will consider shallow foundations and piles as our primary examples and for these foundation types, the idealisations implicit in our methods. We will focus almost exclusively on analysis under undrained conditions, partly because it makes the explanations simpler but partly because it is the more common offshore situation.

We will first consider the analysis and design of shallow foundations.

3. Shallow Foundations

As discussed above there are a number of different offshore applications for shallow foundations and each one brings its own set of issues. In the following we will discuss a number of the design issues and how these can influence the idealisation used in

the analysis and our interpretation of analysis results. We will then briefly discuss conventional analysis methods leading up to more detailed discussions of plasticity analysis methods for situations that fall outside the realm of classical methods.

3.1 Practical issues for designing offshore shallow foundations

3.1.1 Strength Characterisation

One of the primary inputs to any capacity calculation is the soil strength profile. Typical offshore strength profiles are soft clays although sands and overconsolidated clays are also encountered. Of course the strength characterisation must be consistent with the method selected for analysis. The issues that must be addressed include:

- Is the relevant strength characterisation drained or undrained behaviour? This will of course depend on the load characteristics and the drainage conditions in the soil and at soil-foundation interfaces.
- What is the resolution of the site investigation? Site investigations for pile founded structures sometimes have rather coarse sampling intervals so that associated shallow soil profiles may have significant uncertainty in the region critical to shallow foundation performance.
- Is the strength profile best idealised as uniform, linearly increasing, layered or…? Conventional bearing capacity formulae are based on uniform strength profiles. Limited analytical solutions for non-uniform profiles are also available and of course numerical solutions such as finite element methods are capable of analysing very general profiles.
- What is the interface soil strength? There is almost always a thin veneer of very weak soil right at the mudline such that a flat plate placed on this layer would have little sliding resistance under undrained conditions. This often suggests the need for skirts or at least assessing how much the interface strength will improve due to consolidation?
- Will the soils be subjected to cyclic loading? How will the strength profile be modified to account for this?
- Is scour an issue? Can scour undermine the foundation or reduce its effective embedment?

3.1.2 Load Characterisation

The load characteristics also have a significant influence on problem idealisation. The issues that must be addressed include:

- Is the foundation subjected to multi-axial loading? The primary load of interest is often a vertical load but modifications to analysis methods can account for lateral and moment loading as well. Torsional loading is a case that needs special treatment.
- How do the loads vary with time? Are the loads of short duration such as wave or earthquake loading or are the loads sustained?
- Is part of the foundation subjected to uplift loading? Will the foundation have to be removed after its use? If so how will the suction be broken?
- Is the foundation to be placed on a slope which would result in increased lateral loading and overturning?
- If skirts are employed, is the self weight of the structure at installation adequate to achieve full penetration?

3.1.3 Foundation Geometry

The foundation geometry will clearly influence the methods of analysis. Issues include:

- What is the foundation shape? Analytical solutions are mostly limited to strip footings and circular footings. Empirical adjustments are required for rectangular footings. Other shapes have to be treated as special cases.
- Does the foundation have skirts? When skirts are included, conduits are required to allow water to escape from the skirt compartment during placement on bottom.
- Does the foundation have holes in the base to reduce consolidation times? Further, holes can squeeze out some of the soft soil at the interface and also reduce the time required to relieve suction forces if foundation removal is required.
- Is the foundation a single footing or a system of footings such as a mudmat system for a platform? Designing a foundation within a system of footings requires consideration of the system as a whole. For example the system performance will affect the loads that are applied to any individual footing.

The above are some of the considerations that should be taken into account when developing a model for analysing a shallow foundation, carrying out the calculations, and interpreting the results.

3.2 Conventional Methods

3.2.1 Theory

In this section we will discuss conventional bearing capacity equations as well as “exact” solutions to idealised conditions. The development of classical methods for assessing the bearing capacity of shal-

low foundations is built on Prandtl's solution (1921) for a strip footing on the surface of a weightless, frictional material with cohesion and the extension by Reissner (1924) which adds the effect of surcharge to Prandtl's solution. Although we are concentrating on undrained behaviour, the relevant solution is a subset of the general frictional models and hence friction will have to be briefly considered. Prandtl developed his solution from first principles for the two dimensional problem of a strip footing. The two dimensional governing differential equations of equilibrium provide two equations in three unknowns: normal stresses σ_x and σ_y and the shear stress τ_{xy} as shown in Figure 7.

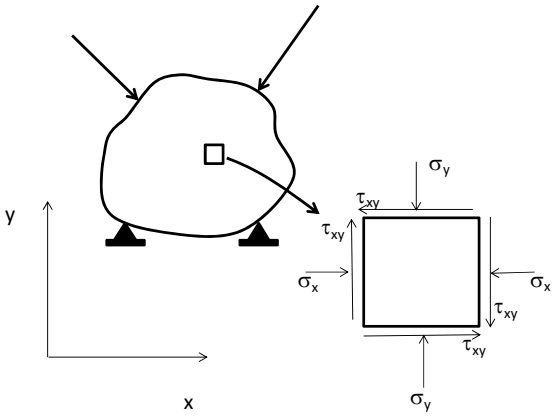

Figure 7: General stress state in a body under load

The required third equation is the yield condition for the material, in this case the Mohr-Coulomb failure criterion:

$$\left(\frac{\sigma_x - \sigma_y}{2}\right)^2 - \tau_{xy}^2 = \frac{\sin^2(\phi)}{4}\left(\sigma_x + \sigma_y + 2c\cot\phi\right)^2 \quad (1)$$

The solution is normally written in the form:

$$V/_A = cN_c + qN_q \quad (2)$$

where V is the total vertical capacity per unit length, A is the footing area per unit length, c is the soil cohesion, q is the effective surcharge pressure at the level of the footing-soil interface, and N_c and N_q are dimensionless functions of soil friction angle, ϕ. Note that for a material with no cohesion and no surcharge the theoretical bearing capacity for the weightless material is zero. The forms of the functions, N_c and N_q, are well documented in the literature, for example see API RP2A. For the special case of $\phi = 0$ i.e. undrained loading, we substitute s_u for c to denote undrained shear strength. For this case the solution is $N_c = 2 + \pi$ and $N_q = 1$. Figure 8 shows one of the possible failure mechanisms corresponding to the characteristic stress solution (although mechanisms are not necessarily unique, the calculated capacity is) for the undrained solution. The solution shown consists of rigid 45°, right triangular wedges beneath the footing and along the free surface. The transition zone between the two is a radial shear fan in which the radial velocity is zero and the angular velocity v_θ is constant. As we will see in a subsequent section, elements of this solution are useful in constructing approximate solutions to more complex problems.

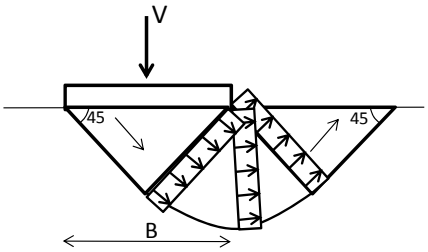

Figure 8: Conventional bearing capacity failure mechanism

The Prandtl equations have been modified to include a semi-empirical term to account for the added strength of the soil due to self-weight such as proposed by Terzaghi (1943) giving:

$$V/_A = cN_c + qN_q + 0.5\gamma BN_\gamma \quad (3)$$

where γ is the effective unit weight, B is the footing width, and N_γ is a dimensionless function of ϕ. Terzaghi also used a value of 5.7 for N_c rather than the theoretical solution, 5.14. The term N_γ was not rigorously derived but was based on adhoc assumptions regarding the stress conditions within the failure mechanism resulting from soil self weight. There are numerous values for the N_γ term found in the literature (Vesic 1972) and because of the sensitivity to friction angle the value of the N_γ term varies widely. Clearly the self weight term in the equation becomes relatively more important as the width of the footing increases. Terzaghi (1943) also modified the equation to account for embedment and the shape of the foundation and various other corrections for these effects have also been published, e.g. Brinch Hansen (1970) and Meyerhof (1953).

A number of modifications to the classical equation have been made by subsequent workers in the field to include the effects of lateral loading and overturning moment. Using Prandtl's approach, Green (1952) derived a rigorous solution to the problem of inclined loading of a rigid punch (footing) on a purely cohesive material (undrained strength) as follows:

$$V/A = s_u[1 + \pi - 2\omega + \cos(2\omega)] \quad (4)$$

where:

$$\omega = \frac{1}{2}\sin^{-1}\left(\frac{\tau}{s_u}\right) \quad (5)$$

where τ is the average shear stress, H/A, where H is the lateral load. Figure 9(a) shows the failure mechanism corresponding to this solution and Figure 9(b) shows the normalized V vs. H interaction diagram. Figure 9(b) also shows the interaction diagram for a case with increasing soil strength as will be discussed later.

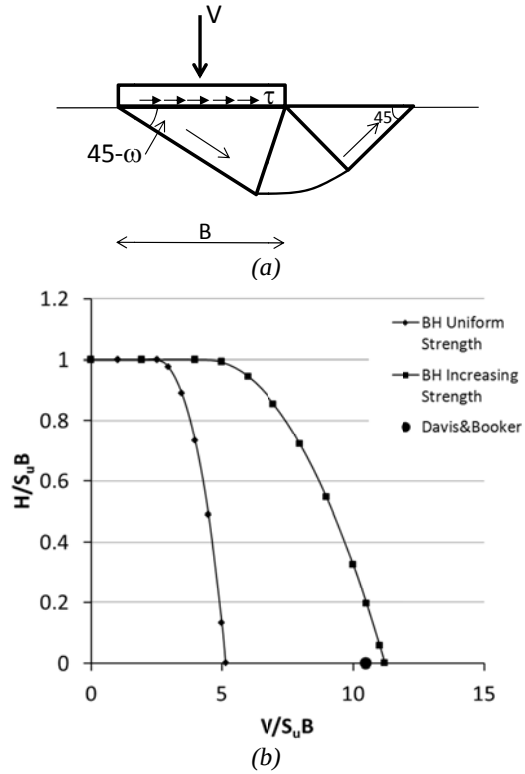

Figure 9: Green's solution (1955) for footing under inclined load (a)mechanism (b)interaction diagram

Note the similarities to the mechanism for pure vertical load. Meyerhof (1953), Brinch Hansen (1970), Vesic (1975), and others have proposed load inclination correction factors that approximate the behaviour of this solution. This solution satisfies equilibrium within the mechanism but according to Houlsby and Puzrin (1999) the stress state has never been extended into the rigid region which is required to be considered a complete solution. Interestingly it can be shown to be an upper bound as will be demonstrated in a subsequent section.

In cases where moments are applied to the footing, the eccentricity or effective offset of the vertical load, e, is:

$$e = M/Q \quad (6)$$

To account for this effect, Brinch Hansen (1970) proposed that the footing area be reduced such that the centroid of the effective area of the reduced footing is at the point of action of the equivalent offset vertical load. An example of this modification is shown in Figure 10. This is a conservative approximation as it satisfies conditions for a lower bound solution, that is, it satisfies equilibrium and can be shown to be at or below yield.

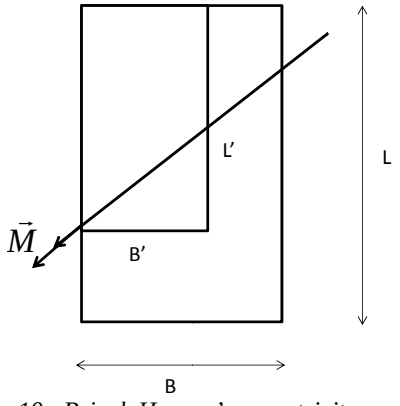

Figure 10: Brinch Hansen's eccentricity correction

Subsequent to the publication of these solutions a number of "exact" solutions have been found using finite difference techniques to integrate the two dimensional governing equations. Sokolovskii (1965) published a book of such solutions including problems of bearing capacity, retaining walls and slopes under varying boundary conditions. Cox, et al. (1961) published solutions for the bearing capacity of a circular footing on the surface of a weightless, Mohr-coulomb material. This was extended to include materials with weight by Cox (1962).

In 1973, Davis and Booker published a finite difference solution to the problem of undrained bearing capacity of a strip footing on the surface of a soil with increasing strength with depth. The solution was presented in the following form:

$$Q/A = F\left[(2 + \pi)s_{uo} + \frac{kB}{4}\right] \quad (7)$$

where s_{uo} is the soil strength at the surface (footing soil interface), k is the rate of increase in undrained strength with depth, and F is a dimensionless function of the parameter kB/s_{uo}. This solution explicitly describes the important effect of the strength gradient on the unit bearing capacity. For example it shows that a wider footing will have higher unit capacity since the failure mechanism is forced deeper into the soil where the strength is greater.

A number of empirical modifications to the above solutions to account for real world complexities have been published. For example, various solutions for layered soils such as a soft layer overlying a hard layer (Brown and Meyerhof, 1969) or sand over clay (Hanna and Meyerhof, 1980) are available to revise designs as required.

3.2.2 Applications

Probably the earliest applications for bearing capacity theory in the offshore were for designing mudmats, the temporary footings used to support a fixed bottom SPJ prior to placement of the piles. The first edition of the API recommended practice, RP2A has a very simple section which provides formulae for the vertical capacity of a surface footing on clay and sand. For example the first edition (October 1969) of RP2A for "mats and spread footings" on clay states, in its entirety:

"The ultimate vertical bearing capacity, q, of clay shall be resolved by the equation:

$$q = 7.4c + p_o \quad (8)$$

where c is the undrained shear strength of clay and p_o is the effective overburden pressure."

There are several things to note regarding this recommendation.

- The equation was intended for vertical load only and hence was intended only for support of the SPJ's on-bottom weight. It does not take into account the lateral and overturning loads that are likely to occur even in a mild environment when an "operational" storm occurs before the piles can be installed. There is no reference to sliding stability under lateral load. SPJ mudmats were generally flat, steel or timber mats that sat directly on the unprepared seabed. As such the sliding resistance of the mats was almost negligible. Figure 11 shows typical mudmat layouts for SPJs. Probably the reasons there were not more incidents of sliding off station were the lateral resistances of partially penetrated horizontal members at the mudline and the extensions of structure legs, called leg stubs, that typically penetrate into the soil several feet.

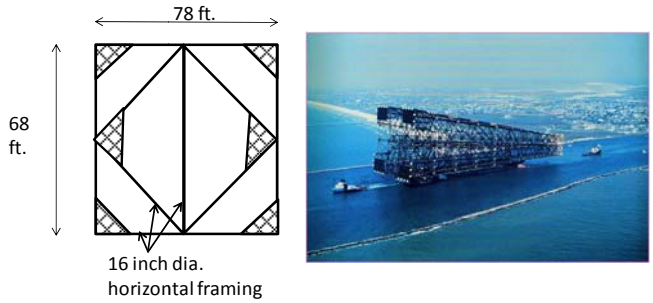

Figure 11: Mudmat layout for steel piled jacket (a) schematic of shallow water platform mudmats (b) deeper water mudmats

- The factor 7.4 is the product of 5.7 (Terzaghi's strip footing factor) and 1.3, Terzaghi's shape factor for a square or circular footing, that is, the provision implicitly assumes the mat shape. This version is somewhat unconservative as the bearing capacity factor is high and a rectangular vs. strip footing shape is implicitly assumed.
- The equation is for a uniform strength soil profile and does not account for the more typical offshore case of an increasing strength with depth. The engineer was faced with picking an appropriate shear strength whereas no guidance is offered in RP2A.
- The RP prescribes a factor of safety of 2.0. One issue that immediately arises is the possibility that the mats will penetrate slightly into the seabed because of the weak soils that are typically found on the seabed. Oftentimes the strength selected was taken from shallow samples that were first, not representative of the increasing strength profile and second, probably disturbed as near mudline samples tended to be. This combination of safety factor and very conservative strength assessment sometimes led to excessively large mudmats and in fact cases occurred where the entire base of an SPJ was one continuous mat.
  This problem arises when the recommended safety factor is taken literally. In this case no penetration of the mats was allowed since if a mat penetrated it was by strict definition at a safety factor of 1.0. As a practical matter however small penetrations are not particularly harmful where the strength gradient is significant as the increasing strength profile tends to be a self correcting feature of the system. In this case it is often possible to bound the potential penetration and judge whether that is an acceptable outcome.
- The equation is intended for a single footing only, not for a system of footings.

RP2A also had a brief section for footings on sand which has many of the same issues. These two sections comprised the only guidelines for shallow

foundations and remained unchanged through several editions. Again no provisions were made for sliding stability. A more comprehensive section for shallow foundations was finally added to RP2A in the tenth edition published in March 1979. In this edition the guidelines published by Vesic (1972) in the Foundation Engineering Handbook were the primary source and included most of the classic bearing capacity concepts discussed above including independent checks for sliding stability. These additions were still intended primarily for the design of SPJ mudmats but their addition was inspired by the introduction of gravity based structures (GBS) in the North Sea in the decade of the 1970s.

As discussed earlier the GBS is a large diameter structure that is especially suited for the hard, flat sea beds in parts of the central North Sea. For most of these structures the controlling design loads are lateral loads such that the critical failure mechanism is sliding. As such the importance of establishing an accurate soil strength profile near the seabed became apparent and one of the key innovations was the addition of skirts to the base of the structure. These skirts were usually thin steel sheets that penetrate vertically into the seabed, typically one to three metres in length, and provide a positive shear connection with the sea floor. The addition of skirts to the base of a mat was not without precedent. For example, some mat-type jack-up rigs have skirts but these are usually limited to the periphery of the mat. As such they add some passive resistance but do not necessarily force a sliding failure on a plane through the skirt tips. An example of a skirted mat is shown in the schematic in Figure 12. The skirts are arranged in a grid pattern on the base of the structure with the spacing of the grid small enough to ensure the critical sliding mechanism is at the tips of the skirts. This recognition of the need for skirts to develop lateral resistance had a carryover effect for other shallow foundations such as mudmats that were to be placed on an unprepared seabed in other offshore developments and is an important design element today. A discussion of the importance of skirts was included in the 10th edition of API RP2A.

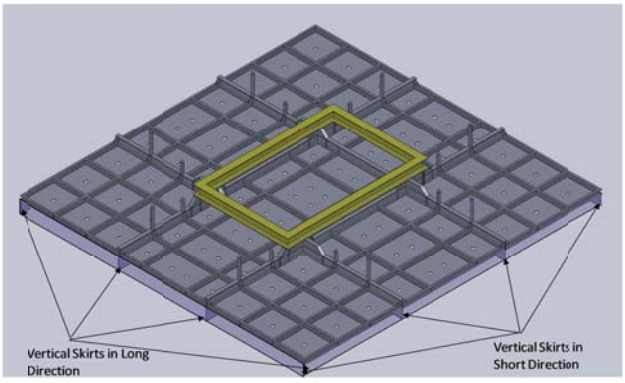

Figure 12: Schematic of shear skirts

The shallow foundations additions made in the 10th Edition of RP2A have been maintained with minor revisions to the present day 21st Edition. However very recently a separate publication, RP2 GEO has been published which provides significantly more detail on foundation design. This document is intended to support various API publications regarding offshore systems such as RP2A (fixed bottom structures), RP2SK (Moorings), and RP2T (TLP foundations). An excellent detailed description of RP2 GEO including a detailed background was published by Jeanjean, et al. (2011).

3.3 Plastic limit analysis – detailed mechanisms

In this section we will discuss methods for analysis of shallow foundation using plastic limit analysis. Such techniques are approximate methods which are less rigorous than the exact characteristics solutions but much more flexible in their ability to address more complex problems such as non-homogeneous soils, multi-axial loading, foundation embedment, etc.

3.3.1 Theory

Plastic limit analysis for this discussion refers to the upper and lower bound theories of plasticity. The upper bound method is much more flexible and easier to apply than the lower bound method and hence will be the primary topic of discussion. It has the added advantage of sharing many of the attributes of the so called limit equilibrium method which is the geotechnical engineer's traditional approach to solving capacity problems. The bound theorems were elucidated by Drucker, et al. (1952). A version of the upper bound theorem due to Calladine (1969) is as follows:

"If an estimate of the plastic collapse load of a body is made by equating internal rate of dissipation of energy to the rate at which external forces do work in any postulated mechanism of deformation of the body, the estimate will be either high or correct."

This requires that we (1) construct a possible collapse mechanism that is kinematically admissible (satisfies the volumetric constraints within the body i.e. the material does not separate or penetrate other material and satisfies the velocity boundary conditions); (2) derive a virtual work equation by setting the work rates of external loads to the internal energy dissipation rates (EDR) within the body; (3) solve the equation for the unknown external load or scale factor for a load envelope; and (4) repeat the process varying geometric parameters (if any) describing the mechanism to find the minimum collapse load for that mechanism.

The validity of the bound theorems is dependent on the following standard assumptions of plasticity theory.

- The yield surface, $f(\sigma_{ij}) = 0$, is convex in stress space.
- Principal stresses and principal strain rates are aligned in stress space.
- Plastic strain increments, $\dot{\varepsilon}_{ij}$, are normal to the yield surface such that:

$$\dot{\varepsilon}_{ij} = \lambda \frac{\partial f}{\partial \sigma_{ij}} \tag{9}$$

where λ is a positive scalar. This equation is somewhat abstract and I have found students have difficulty visualizing its meaning. Conceptually it means that the stresses that brought the material to yield are the ones that control the strain directions. For example consider Figure 13 which shows a simple schematic of a yield surface in two dimensional stress space.

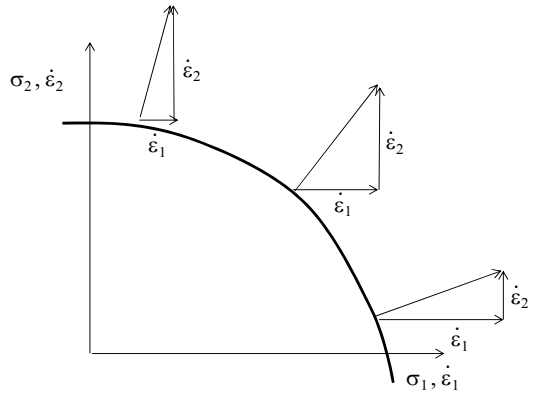

Figure 13: Schematic of yield surface showing normality of strain increments

As shown, if the stress state is primarily σ_1 the primary strain direction is in the $\dot{\varepsilon}_1$ direction and likewise for other stress states. Since the material stress-strain behaviour is non-linear and history dependent it is only possible to determine the strain increment directions independent of the overall boundary value problem solution. For a given point on the yield surface it is possible to determine the relative values of the strain increment components, for example:

$$\frac{\dot{\varepsilon}_x}{\dot{\varepsilon}_y} = \frac{\partial f / \partial \sigma_x}{\partial f / \partial \sigma_y} \tag{10}$$

since the scalar λ cancels in the ratio. There are two possible modes of deformation in a plastically deforming material: tangential slip along a failure surface or slip plane and continuous deformation in the plastic continuum. The EDR referred to in the upper bound theorem can be expressed in terms of strain increments for a given yield condition as demonstrated, for example, by Drucker and Prager (1952). They derived the dissipation rates for a generalized von mises yield condition for a frictional material with cohesion. Such dissipation equations have been derived for materials obeying other yield conditions. Of particular interest for the purposes here is the Tresca or maximum shear stress criterion for a purely cohesive material. The dissipation equations for this material for the two failure modes is

$$\textit{Slip on a failure surface:}\quad \dot{D} = s_u v_r \tag{11}$$

and

$$\textit{Continuous deformation:}\quad \dot{D} = 2 s_u |\dot{\varepsilon}|_{max} \tag{12}$$

where v_r is the relative slip velocity on the failure plane, s_u is the undrained shear strength, and $|\dot{\varepsilon}|_{max}$ is the absolute value of the numerically largest principal strain increment. These equations allow us to calculate the energy dissipation rate for any admissible failure mechanism using virtual work principles.

Before discussing applications we should point out that there are a number of corollaries to the bound theorems that can be extremely useful as discussed by Chen (1975). Two of these are particularly important and warrant a brief mention here as follows,

- The plastic collapse load of a system of perfectly plastic elements is independent of the elastic behaviour of the material as long as any deformation does not significantly change the original geometry.
- Removing (adding) a constraint from a system of perfectly plastic elements cannot make the system stronger (weaker).

One of the requirements of a perfectly plastic system is that the material remains stable i.e. does not exhibit strain softening.

3.3.2 Applicatons

Perhaps the best way to explain the upper bound method is to provide an example of an application.

Example 1

Consider the mechanism shown in Figure 14 for a footing subjected to an inclined load. This is similar to the mechanism corresponding to Green's (1952) solution, shown in Figure 9(a), except that the angle θ is assumed to be unknown. The solution for V, for the upper bound formulation, is then minimized by varying θ.

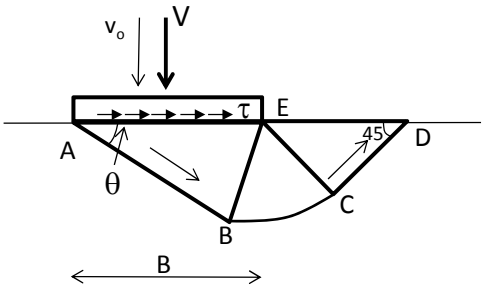

Figure 14: Inclined load failure mechanism

We begin by assuming a virtual velocity in the downward vertical direction. To be admissible the footing and soil wedge must slide parallel to surface AB so that the total dissipation along AB is

$$\dot{D}_{AB} = v_{AB} * l_{AB} * \mathrm{s_u} = \frac{v_o}{\sin\theta} * s_u * B\cos\theta$$

$$= v_o s_u B\cot\theta \tag{13}$$

where the parameters are as previously defined and/or shown in Figure 14. At interface BE, the soil moves uniformly to be compatible with wedge ABE so that the dissipation along curve BC is

$$\dot{D}_{BC} = \frac{v_o}{\sin\theta} * s_u * \left(\frac{\pi}{4}+\theta\right) B\sin\theta$$

$$= v_o s_u B\left(\frac{\pi}{4}+\theta\right) \tag{14}$$

At interface EC, the soil again must move uniformly so that the dissipation along CD is

$$\dot{D}_{CD} = \frac{v_o}{\sin\theta} * s_u B\sin\theta = v_o s_u B \tag{15}$$

The sector BCE is a radial shear fan centred at E. To be compatible with the other parts of the mechanism the radial velocity must be zero and the tangential velocity is $v_\theta = v_o/\sin\theta$, a constant. This is the only continuously deforming region. The only non-zero strain rate is

$$\dot{\varepsilon}_{r\theta} = \frac{1}{2}\left(\frac{\partial v_r}{r\partial\theta} + \frac{\eth v_\theta}{\partial r} - \frac{v_\theta}{r}\right) = \frac{-v_o}{2r\sin\theta} \tag{16}$$

The maximum principal strain rate is then

$$|\dot{\varepsilon}|_{max} = \frac{v_o}{2r\sin\theta} \tag{17}$$

and the resulting dissipation rate is

$$\dot{D}_{BCE} = \int_0^{B\sin\theta}\int_0^{\frac{\pi}{4}+\theta} \frac{s_u v_o}{r\sin\theta} r d\theta' dr$$

$$= v_o s_u B\left(\frac{\pi}{4}+\theta\right) \tag{18}$$

The external work rate is the sum of the rates of both the vertical force component, V, and the horizontal component, H. We replace the horizontal force with the average shear stress, τ, times the footing width, B, to give

$$\dot{W} = V v_o + \frac{H v_o}{\tan\theta} = \left(V + \frac{\tau B}{\tan\theta}\right) v_o \tag{19}$$

Setting the work rate equal to the sum of the dissipation rates, cancelling v_o, solving for V and simplifying gives

$$V = B s_u\left[\frac{\pi}{2} + 2\theta + 1 + \cot\theta\left(1 - \frac{\tau}{s_u}\right)\right] \tag{20}$$

Now minimizing V with respect to θ gives

$$\frac{\partial V}{\partial\theta} = B s_u\left[2 - \csc^2\theta\left(1 - \frac{\tau}{s_u}\right)\right] = 0 \tag{21}$$

Solving gives the critical value of θ

$$\theta = \frac{1}{2}\cos^{-1}\frac{\tau}{s_u} \tag{22}$$

Recognizing that $\theta = (\pi/4) - \omega$, Equations 4 and 20 are identical. It is interesting that the solution developed from equilibrium arguments has not been proved a lower bound but can be shown to be an upper bound. It should also be noted that components of the mechanism used in this example can often be used to build mechanisms for other problems. For example for a footing with a small aspect ratio, $L/B < 2$, a three dimensional approximation can be achieved by assuming a vertical failure plane at each end of the footing. This requires integrating the EDR over the resulting slip surfaces and adding to the total dissipation.

It should be recognized that the mechanism in this solution results in vertical and horizontal translation only. Since there is no provision in the mechanism for rotation, the solution will not be affected by a moment included in the loads. Since there is no rotation, the moment would do no work and hence this solution would tell you nothing about the effects of moment. It is, however, relatively easy to modify the mechanism to include rotation as will be shown in the next example. We can also include non-homogeneous strengths in the solution by expressing shear strength as a function of depth in the dissipation terms and integrating over the various slip surfaces and the radial shear fan as will be discussed below.

Example 2

A proposed mechanism to include moment effects is shown in Figure 15. Moments can arise due to an elevated horizontal load, an eccentric vertical load, and/or a moment couple. The solution shown in Figure 15 was proposed by Brinch Hansen (1970) and formulated as an upper bound mechanism by Murff and Miller (1977a). The coordinates, x_o and y_o, of the centre of rotation of the mechanism are the optimization parameters and are varied to find the least upper bound. Note that there are slightly different mechanisms for $x_o < 0$ and $x_o > 0$ which are continuous at the $x_o = 0$ transition. It is assumed for $x_o < 0$ that the footing stays attached to the soil so there is no separation of the footing from the soil along AE.

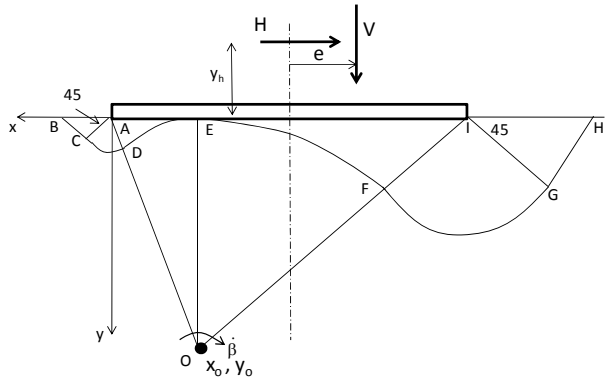

Figure 15: Eccentric load failure mechanism

Consider now some details of the mechanism. R_1 is the distance OE; R_2 is the distance OI; and R_3 is the distance OA. The footing rotates about x_o, y_o at a virtual angular velocity of $\dot{\beta}$. The failure mechanism in the soil on the left of OE is similar but of different dimensions than the one to the right of OE. The sectors EFI and EDA are non-deforming elements. Sectors FGI and DCA are radial shear fans but, in this case, the tangential velocity varies with the radius to be consistent with the velocities along FI and DA. The wedges GHI and CBA deform and slip along the boundaries GH and CB. In general, the loads are taken as a vertical load, V, offset a distance e from the footing centre and a horizontal load, H, at a height y_h above the footing base. Both V and H can contribute overturning moments and of course a moment couple can also be applied.

To carry out the calculations local coordinate systems are used to simplify the process. In the general cases, integrations are carried out along slip surfaces and within deforming regions to get the respective EDR values. For varying strengths with depth the shear strength profile has to be expressed in terms of the local coordinate system used for the calculation. These calculations are somewhat tedious so examples for typical components are detailed in Appendix I. The total EDR is determined simply by summing the components.

The external work rate is then given by the following

$$\dot{W}_e = \left[H * (y_h + y_o) + V * \left(x_o + \frac{B}{2} + e\right)\right]\dot{\beta} \qquad (23)$$

Following the upper bound procedure we then set the total work rate to the total EDR

$$H * (y_h + y_o)\dot{\beta} + V * \left(x_o + \frac{B}{2} + e\right)\dot{\beta} = \sum_{i=1}^{n} \dot{D}_i \qquad (24)$$

Now $\dot{\beta}$ appears linearly in each term of the equation and is cancelled as the virtual work method dictates. One can then decide which load, H or V, is of interest, specify the other, and solve for the one of interest. For example say the vertical load V is the known dead load on the footing and H is the lateral capacity of interest. The solution for the lateral capacity estimate is then

$$H = \frac{\sum_{i=1}^{n} D_i - V\left(x_o + \frac{B}{2} + e\right)}{y_h + y_o} \qquad (25)$$

Note that D is now specified without the dot indicating the virtual velocity, $\dot{\beta}$ values, have been cancelled. H is then minimized with respect to the coordinates x_o, y_o to find the least upper bound.

This mechanism accounts for effects of V, H, and M and their interactions and we can plot the full VHM surface using these equations. More typically we

plot two dimensional interactions such as H vs. V, H vs. M, or M vs. V however in these cases it must be kept in mind that these plots are cross sections of the overall surface and such plots can be significantly affected by the third load component. The question that then arises is how good are these solutions, especially since they are upper bounds and hence they are on the unconservative side.

For the linearly increasing strength cases ($kB/s_{uo} = 6$), Figure 9(b) shows that the vertical capacity results are quite good. Clearly the horizontal capacity is exact as well and hence it is likely that the interaction curve is near the exact one as it is for special case of uniform strength. However for VM and HM interactions, experience has shown that this mechanism significantly over predicts some parts of the yield surface. For example for small vertical loads, Gourvenec and Randolph (2003) have shown that the simple scoop mechanism, as shown in Figure 16 works well. On the other hand, the scoop over predicts for large vertical loads. Consider the details of the scoop mechanism.

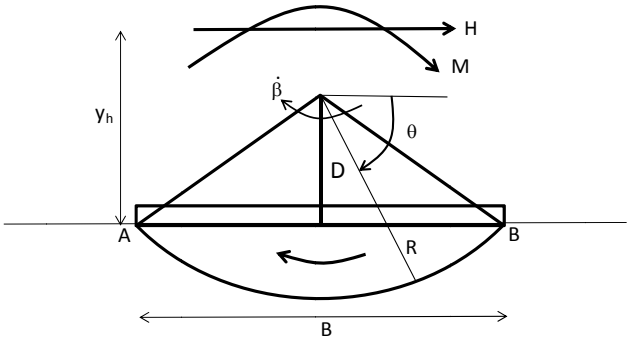

Figure 16: Scoop failure mechanism

The distance D, from the assumed centre of rotation to the soil surface, is the single optimization variable and the load of primary interest is the total moment at the footing centroid. This includes any directly applied moment plus the lateral load, H, times its height, y_h, above the soil surface. The circular segment AB is rigid and hence the only dissipation is along arc AB as shown in Figure 16. The EDR is simply as follows,

$$\dot{D}_{AB} = 2\dot{\beta}\int_{\tan^{-1}\left(\frac{2D}{B}\right)}^{\frac{\pi}{2}}\left[D^2 + \left(\frac{B}{2}\right)^2\right]^{\frac{1}{2}} s_u(y)d\theta \tag{26}$$

In the general case the depth y for this mechanism is

$$y = \left[D^2 + \left(\frac{B}{2}\right)^2\right]^{\frac{1}{2}}\sin\theta - D \tag{27}$$

Numerical integration can be used for strength profiles that do not permit analytical integration. The external work rate is then set equal to the EDR to give

$$\dot{W} = (H * (y_h - D) + M_c)\dot{\beta} \tag{28}$$

In this case M_c accounts for a couple that may be directly applied to the footing. Either M_c or H can be solved for if the other component is known. For example assume the applied moment, M_c, is known, then H is as follows

$$H = \frac{2\int_{\tan^{-1}\left(\frac{2D}{B}\right)}^{\frac{\pi}{2}}\left[D^2 + \left(\frac{B}{2}\right)^2\right]^{\frac{1}{2}} s_u(y)d\theta' - M_c}{y_h - D} \tag{29}$$

Optimization is then carried out with respect to D.

The foregoing provides two relatively simple models that provide approximate solutions over a range of loads. Consider some specific results for the two mechanisms. The BH mechanism gives good results for VH interaction for example, it converges to Green's solution (1952) for $M = 0$. Figure 17 and Figure 18 show results for the two failure mechanisms for MV and MH interactions respectively for the uniform strength case and for the case of increasing strength with depth ($kB/s_{uo} = 6$). Also shown in these figures are the results scaled from the plots shown in the paper by Gourvenec and Randolph (2003) referred to here as GR. The GR results are based on more detailed mechanism studies combined with finite element results and are believed to be very close to exact solutions.

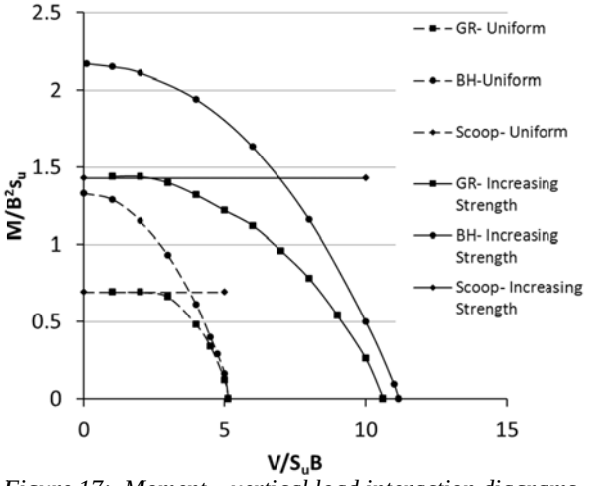

Figure 17: Moment – vertical load interaction diagrams

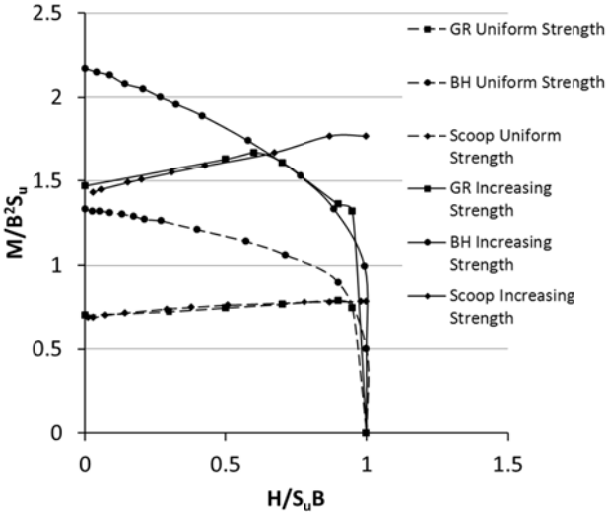

Figure 18: Moment – horizontal load interaction diagrams

For vertical load vs. moment interaction ($H = 0$) the BH mechanism only captures the moment effects well for relatively large values of vertical load. On the contrary, the scoop mechanism does well on the other end of the vertical load scale- in fact the scoop results are independent of centric vertical load. More significant errors are apparent for midrange vertical load values. The largest errors are for the increasing strength case and these can be improved somewhat by simply correcting the vertical capacity components by the known over prediction of the pure vertical load case, 7.2% in this case as shown in Figure 9(b).

For horizontal load vs. moment interaction ($V = 0$) the BH mechanism only does well for horizontal loads near sliding for the uniform strength case but does somewhat better for the increasing strength case ($kB/s_{uo} = 6$) down to near midrange. The scoop mechanism does surprisingly well over almost the entire range of horizontal loads. The combination of the two mechanisms is almost an exact fit to the GR results. As was pointed out by Bransby and Randolph (1996) and emphasized by Gourvenec and Randolph (2003), it is quite interesting that horizontal load in the direction of increasing moment actually increases the moment resistance up to a value of $H/s_{uo}B$of about 0.6.

The foregoing results underscore the importance of validating solutions based on assumed mechanisms but also show that some relatively simple mechanisms can give good results to complex problems. Hopefully these results provide a bit of insight into how one might go about developing approximate solutions and sufficient detail regarding the mechanics of the calculation procedures. In the next section we will discuss some additional strategies for finding mechanisms for various shallow foundation problems.

3.3.3 Additional Strategies

We have seen that mechanisms can be constructed from components that are found in classical solutions such as slip circles, radial shear fans, and rigid or deforming wedges. The intention of the following discussion is to provide further insight into constructing mechanisms by providing examples of strategies that can be used to advantage.

The Squeeze Problem

We have previously shown that the yield condition for undrained strength (purely cohesive behaviour) implies that the plastic deformation will be incompressible. Since this constraint is necessary it can actually aid us in constructing a velocity field for a particular mechanism.

Figure 19 is a schematic in which a strip footing is placed on a soft, relatively thin, uniform layer overlying a hard stratum.

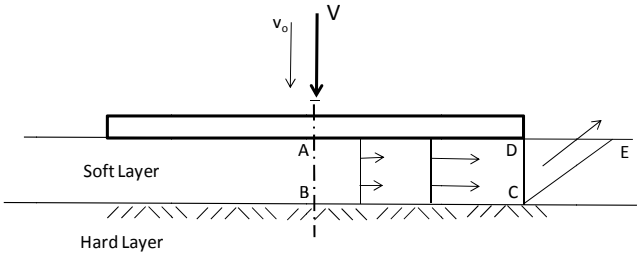

Figure 19: Schematic diagram of a proposed squeeze mechanism

At the footing interface we can expect the soil to move downward and to be squeezed outward. At the interface between the soft layer and hard stratum the vertical movement of the soil would presumably be zero. Since we know that the vertical velocity must vary from v_o at the footing interface to zero at the hard stratum interface, a simple assumption is that the variation is linear, that is

$$v_y = v_o(1 - y/t) \tag{30}$$

We further assume that v_y is not a function of x. We can then find a v_x that "works" by exploiting the incompressibility condition as follows,

$$\dot{\varepsilon_v} = \dot{\varepsilon_x} + \dot{\varepsilon_y} = \frac{\partial v_x}{\partial x} + \frac{\partial v_y}{\partial y} = 0 \tag{31}$$

This results in the differential equation

$$\frac{\partial v_x}{\partial x} - \frac{v_o}{t} = 0 \tag{32}$$

Integrating this equation yields the simple solution

$$v_x = \frac{v_o x}{t} + f(y) \tag{33}$$

Applying the boundary condition (symmetry), $v_x = 0$ at $x = 0$, the function $f(y)$ must be zero and hence the strain rates are

$$\dot{\varepsilon_x} = \frac{v_o}{t} \quad \text{and} \quad \dot{\varepsilon_y} = \frac{-v_o}{t} \tag{34}$$

The EDR is then

$$\dot{D}_{ABCD} = \frac{2 s_u v_o}{t} \tag{35}$$

Since the EDR is a constant throughout the region ABCD, the total dissipation rate is simply

$$\dot{D}_{ABCD-tot} = \frac{2 s_u v_o}{t} * Volume = s_u B v_o \tag{36}$$

To complete the solution we must include EDRs at the footing-soil interface AD (unless we assume the interface is smooth), the soft-hard stratum interface BC, the passive resistance of the wedges CE, and the soil interface CD. Note that the downward velocity of the soil beneath the footing and the upward velocity of the outer wedges give rise to increased relative velocity at interface CD.

Details of these remaining calculations are provided in Appendix II. The failure load assuming interfaces AD and BC are rough is then

$$\frac{V}{B s_u} = 2 + \frac{B}{2t} + \frac{1}{\sin\theta \cos\theta} + \tan\theta + \frac{t}{B} \tag{37}$$

For a smooth footing, the dissipation at the AD interface is set to zero. Results of the capacity as a function of soft layer thickness are shown in Figure 20 for the rough footing case. Since one can construct an upper bound mechanism for a soft layer thickness of $0.35B$ which gives the classical solution, $2 + \pi$, the squeeze mechanism is 6.61, well above this value. On the other hand it does provide a useful solution in that it demonstrates the effect of thin weak layers in a relative sense. Defining a "scale" factor of $5.14/6.61 = 0.78$ and scaling the ordinates of the squeeze solution gives the corrected plot in Figure 20. This at least gives a "feel" for the effect of thin weak layers.

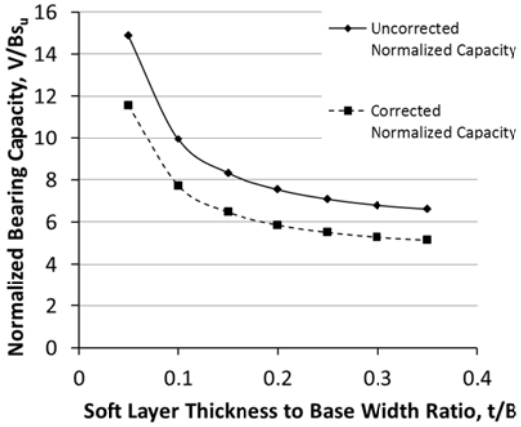

Figure 20: Capacity of footing on thin soft layer with varying thickness

A similar approach can be applied to a circular footing where a cylindrical coordinate system is used. The soil is assumed to deform in an axisymmetric pattern in keeping with the geometry of the problem. Note that following standard convention, z is used here in place of y. Again assuming a linear variation of v_z,

$$v_z = v_o \left(1 - \frac{z}{t}\right) \tag{38}$$

and applying the incompressibility constraint we obtain

$$\dot{\varepsilon}_r + \dot{\varepsilon}_\theta + \dot{\varepsilon}_z = \frac{\partial v_r}{\partial r} + \frac{v_r}{r} + \frac{\partial v_z}{\partial z} = 0 \tag{39}$$

This leads to the equation

$$\frac{\partial v_r}{\partial r} + \frac{v_r}{r} = \frac{v_o}{t} \tag{40}$$

As before v_r is a function of r only. Solving the equation, and applying the boundary condition $v_r = 0$ at $r = 0$, gives the solution

$$v_r = \frac{v_o r}{2t} \tag{41}$$

The strain increments are then

$$\dot{\varepsilon}_r = \frac{v_o}{2t} \qquad \dot{\varepsilon}_\theta = \frac{v_o}{2t} \qquad \dot{\varepsilon}_r = -\frac{v_o}{t} \tag{42}$$

and the EDR per unit volume is

$$\dot{D} = \frac{2 s_u v_o}{t} \tag{43}$$

The total dissipation in the zone below the footing is then the unit dissipation times the volume of the cylinder defining the deforming region. The remainder of the EDR components is calculated in a similar manner to that for plane strain except that the toroidal wedge around the thin zone must deform owing to its axisymmetric geometry. In this case the

circumferential strain is not zero and the velocity fields are again constructed using the incompressibility condition. The details of the calculations are described in the paper by Murff and Miller (1980).

In the foregoing we have attempted to demonstrate some of the thought processes and procedures that can be used for constructing failure mechanisms for upper bound analysis. While the idea of failure mechanisms is familiar to the geotechnical engineer, care must be taken to ensure the mechanisms are kinematically admissible. In a sense this really just means that they are possible. A more detailed discussion of this aspect of limit analysis is provided later.

3.4 Generalised Plastic Limit Analysis – Macro Mechanisms

The foregoing analyses have demonstrated the construction of detailed failure mechanisms to be used in conjunction with upper bound plastic limit analysis. In this section we will consider how failure interaction surfaces can themselves be used to derive the performance of a foundation element. Prager (1959) showed that a system of forces that characterise the stress state in a perfectly plastic structure (including a soil-structure system) can be considered generalized stresses and the corresponding plastic displacements can be considered generalized strains. This is true notwithstanding the fact that the generalised stresses and strains do not have the actual dimensions of stress and strain. For a given set of generalized stresses, $Q_1 \dots Q_n$, the generalized strain rates, $\dot{q}_1 \dots \dot{q}_n$ are the work rate conjugates of the stresses, that is

$$\dot{W} = Q_1\dot{q}_1 + \dots + Q_n\dot{q}_n \tag{44}$$

Where the generalized stresses are moments, the generalized strains are rotations so that work rate conjugancy is maintained. The interaction surface then plays the role of the yield condition, that is

$$f(Q_1, \dots, Q_n) = 0 \tag{45}$$

If the structure is composed of perfectly plastic elements, the yield function, f, is convex and other tenents of plasticity theory apply. As for the plastic stress vs. strain relationships we can relate the generalized plastic strain rates to the generalized yield condition using the associated flow rule, that is

$$\dot{q}_i = \lambda\frac{\partial f}{\partial Q_i} \tag{46}$$

We can then use these elements to apply the bound theorems to any assemblage of generalized plastic elements such as a system of footings or piles.

Before considering relevant problems it is useful to demonstrate the validity of Prager's assertion. Consider the problem discussed earlier of a footing on uniform strength soil subjected to inclined load. Equations 4 and 5 constitute the failure interaction surface which can be rewritten in terms of normalized vertical load V and horizontal load H, that is

$$f(V,H) = \frac{V}{H_{max}} - [1 + \pi - 2\omega + \cos(2\omega)] = 0 \tag{47}$$

where

$$\omega = \frac{1}{2}\sin^{-1}\left(\frac{H}{H_{max}}\right) \tag{48}$$

Now the generalized plastic strain rates corresponding to the generalized stresses V and H are

$$\dot{v} = \lambda\frac{\partial f}{\partial V} = \frac{\lambda}{H_{max}} \tag{49}$$

and

$$\dot{h} = \lambda\frac{\partial f}{\partial H} = \lambda\left[\frac{1 + H_r}{H_{max}\left(1 - {H_r}^2\right)^{\frac{1}{2}}}\right] \tag{50}$$

where H_r is the ratio of H to H_{max}. We can then find the ratio of strain rates,

$$\frac{\dot{v}}{\dot{h}} = \frac{\left(1 - {H_r}^2\right)^{\frac{1}{2}}}{1 + H_r} \tag{51}$$

Consider now a specific example where $V = 0.9V_{max}$ which equals $4.626Bs_u$. Solving for H using the yield equation, $H = 0.4124Bs_u$ and the ratio $\dot{v}/\dot{h} = 0.644$, ω is then found to equal 12.2°. Referring to the failure mechanism in Figure 21, the footing moves downward at an angle of *45°-12.2°=32.8°* to the horizontal giving a ratio of $\dot{v}/\dot{h} = \tan(32.8°) = 0.644$ which checks identically.

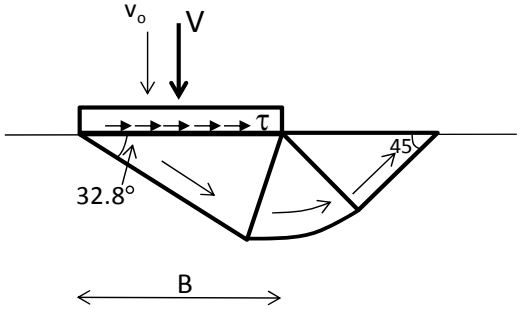

Figure 21: Inclined load failure mechanism showing velocity of footing

Figure 22 shows that the strain increment is indeed normal to the yield surface. Thus for any combination of V and H at yield we can determine the ratio of $\dot{v}/\dot{h}$. Alternatively (and perhaps more importantly) we can invert the process and determine V and H for any ratio of $\dot{v}/\dot{h}$. This may, of course, require solving a non-linear equation but the idea has particular advantages when analysing a mechanism involving a system of foundation elements.

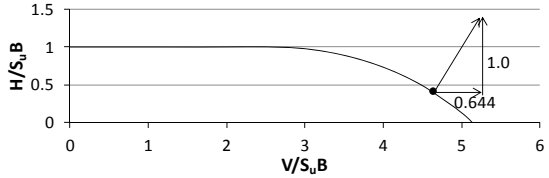

Figure 22: Inclined load interaction surface showing normality of the velocity field

Consider the system of shallow foundations shown in Figure 23(a). One approach to solving the capacity of the system is to construct a mechanism as shown in Figure 23(a) as proposed by Murff and Miller (1977b). A simpler approach however is to represent each footing by its multi-axial interaction diagram as suggested in Figure 23(b). This can be easier and more accurate, especially if we have an accurate interaction surface for a single footing.

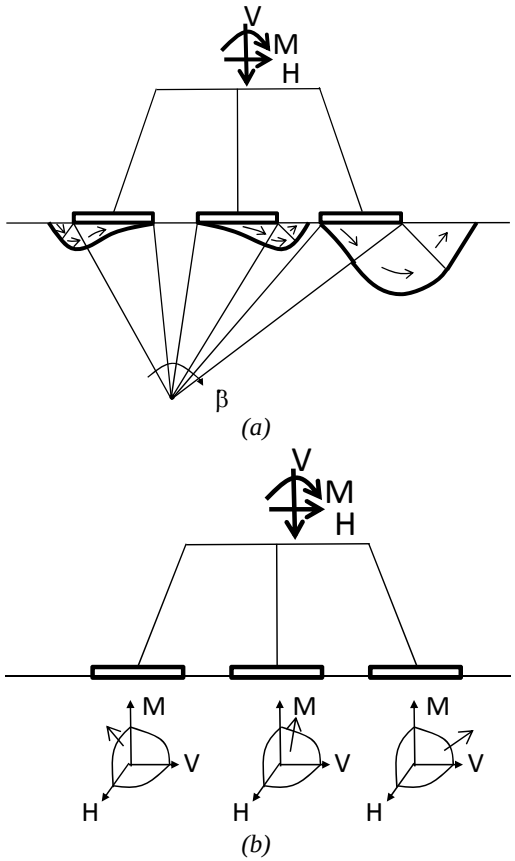

Figure 23: Shallow foundation system (a) detailed mechanism (b) system represented by interaction surfaces

Assume, for example, a yield function, $f(V,H,M)=0$, for a single footing. The following is a step by step approach to determine the system capacity.

1. Assume a virtual rotation of the system about a point with coordinates x_0 and y_0 which become the optimization parameters. For a planar geometry the mechanism represents all possible motions- two translations and a rotation.
2. For any values, x_0 and y_0, find the motion $\dot{v}_i$, $\dot{h}_i$ for the centres of each footing. Note the rotation rate $\dot{\theta}_i$ for all footings is equal to $\dot{\beta}$.
3. Now form the ratios of virtual translation and rotation components, for example

$$\frac{\dot{v}_i}{\dot{h}_i}=\frac{\partial f/\partial V}{\partial f/\partial H} \tag{52}$$

4. Since we know the ratios themselves from the assumed mechanism, this gives us three equations of this type but only two independent ones (any two) in unknowns V, H, and M
5. The third equation needed for solving for V, H, and M for any footing is the yield condition. Thus

in principal we can solve for the three unknowns although, depending on the complexity of the yield condition, this may be numerically difficult.

6. Given the values of V, H, and M we can calculate the EDR for any footing as follows

$$\dot{D}_i = V_i \dot{v}_i + H_i \dot{h}_i + M_i \dot{\theta}_i \tag{53}$$

7. Equating the virtual work rate of the external loads to the EDR we can then solve for the unknown load or scale factor.
8. We then systematically vary x_0 and y_0 to find the minimum load capacity.

In as much as the mechanism is planar and the yield condition of each footing is correct, minimization will lead to the exact solution because we have considered all possible failure mechanisms. In fact since we have calculated V, H, and M at each footing and know the external loads we can check to see whether the solution satisfies equilibrium. We will discuss how to investigate failure out of the plane of loading in our discussion of pile systems. As we did before, we will use an example to demonstrate the above ideas.

Example 3

Here we will consider a simple example of planar failure of a two footing system as shown in Figure 24. For our purposes we will assume that the footings are pinned to the structure at their centroids and the interaction surface is as given in Equations 47 and 48. As noted earlier removing a constraint from a plastic system, such as replacing a rigid connection with a hinge, will never increase the capacity and hence will be a conservative assumption as noted by Chen (1972).

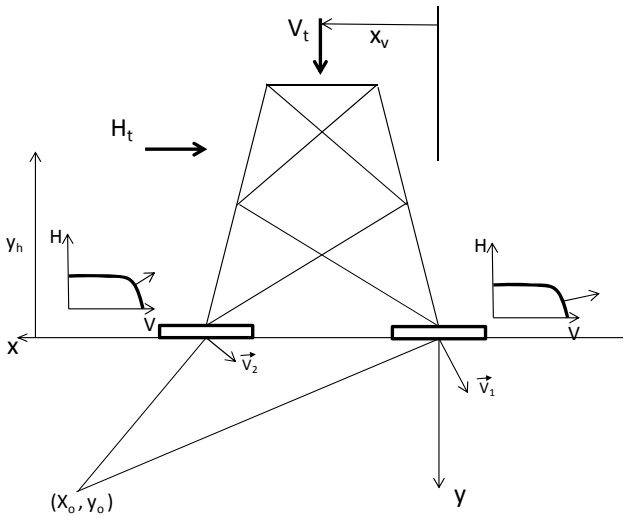

Figure 24: Schematic of two-footing system with loads

The system is subjected to its self weight as well as a lateral load. There are two unknowns associated with each footing, V_i and H_i.

For a given value of x_0 and y_0 the ratio of virtual velocities at each footing is

$$\frac{\dot{v}_{fi}}{\dot{h}_{fi}} = \frac{(x_o - x_{fi})\dot{\beta}}{(y_o - y_{fi})\dot{\beta}} = C \tag{54}$$

where x_{fi} and y_{fi} are the footing coordinates. We also know from the normality relationships that

$$\frac{\dot{v}_{fi}}{\dot{h}_{fi}} = \frac{\lambda \frac{\partial f}{\partial V_{fi}}}{\lambda \frac{\partial f}{\partial H_{fi}}} = \frac{\left[1 - \left(\frac{H_{fi}}{H_{max\,fi}}\right)^2\right]^{\frac{1}{2}}}{1 + \left(\frac{H_{fi}}{H_{max\,fi}}\right)} = \frac{x_o - x_{fi}}{y_o - y_{fi}} \tag{55}$$

The right hand side is known for any value of x_0 and y_0 and hence we can reduce Equation 55 to a quadratic equation of the form

$$H_r{}^2 + \alpha H_r + \beta = 0 \tag{56}$$

where

$$H_r = \frac{H}{H_{max}} \quad \alpha = \frac{2C^2}{C^2 + 1} \quad \text{and} \quad \beta = \frac{C^2 - 1}{C^2 + 1} \tag{57}$$

Solving and taking the positive root (on physical grounds) gives

$$H_r = \frac{-\alpha + \sqrt{\alpha^2 - 4\beta}}{2} \tag{58}$$

Knowing the H_{fi}, we can solve for V_{fi} directly from the yield condition, Equations 47 and 48. The total EDR is then

$$\dot{D}_{total} = \sum_{i=1}^{2} \left(H_{fi} \dot{h}_{fi} + V_{fi} \dot{v}_{fi}\right) \tag{59}$$

As shown in Figure 25 the mathematical interaction equation extends beyond the boundaries of the yield surface.

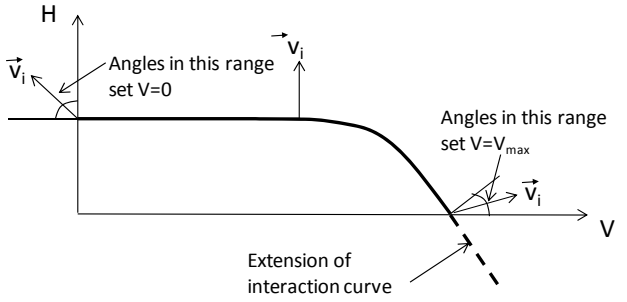

Figure 25: Interaction surface for single footing reset end values

Therefore if V_{fi} or H_{fi} are outside the physically meaningful range we reset them to their boundary values as shown in Figure 25. This adjustment will sometimes lead to an indeterminacy in the footing loads however within the range of acceptable loads, equilibrium can still be satisfied. The total external work rate is then

$$\dot{W} = H * (y_o + y_h)\dot{\beta} + V * (x_o - x_v)\dot{\beta} \qquad (60)$$

Now we can set V or H equal to a specified value such as $V =$ self weight of system, and solve for the other component, for example

$$H_{total} = \frac{\sum_{i=1}^{2}\left[H_{fi}(y_o - y_{fi}) + V_{fi}(x_o - x_{fi})\right]}{(y_o + y_h)} - \frac{V(x_o - x_v)}{(y_o + y_h)} \qquad (61)$$

Figure 26 shows normalized results of moment vs. horizontal load interaction for a system of footings with *2B* centre to centre spacing for a range of vertical loads. For small vertical loads the interaction diagram is rectangular i.e. there is no interaction. The failure mode is sliding for horizontal loads near the mudline or simple overturning for loads at significantly higher elevations. The interaction diagram grows as the vertical load is increased but beyond a certain vertical load it begins to shrink as shown in the figure. Note that it is relatively straight forward to add additional footings to the system using Equations 55 through 58.

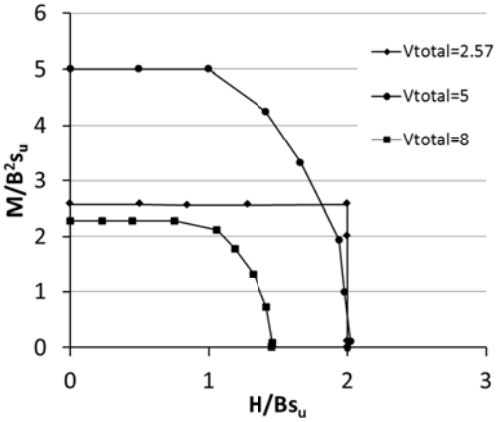

Figure 26: Normalized interaction diagrams for two-footing system for varying normalised load

The foregoing example utilized an exact solution for single foundations in analysing a system. One of the useful features of using macro-mechanisms is that single footing solutions can also include conventional solutions as well as strictly empirical curve fits. One example of the latter is described by Murff (1994). This study involved an empirical equation for the yield function of circular footings of the form

$$\sqrt{\left(M/D\right)^2 + \Lambda_1 H^2} + \Lambda_2\left[\frac{V^2}{V_c} - \left(1 - \frac{V_t}{V_c}\right)V + V_t\right] = 0 \qquad (62)$$

where Λ_1 and Λ_2 are fitting parameters and V_c and V_t are pure compression and pure tension capacity of each footing, respectively. As described in the paper, Equation 62 is a mathematically tractable form so that a spreadsheet can be used to develop system interaction diagrams using the procedures outlined above. Details of the analysis are described in the paper. Another option is to use conventional bearing capacity equations as yield conditions. Figure 27 shows examples of conventional "inclination" factors that are used to modify the basic bearing capacity equations for a strip footing on clay. All three conventional factors are reasonable matches to Green's exact solution and could be used to approximate system behaviour.

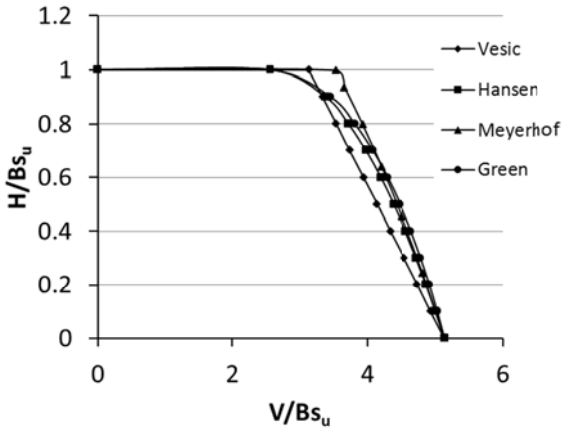

Figure 27: Empirical interaction surfaces compared with Green's solution

It is noted however that Vesic's correction is composed of straight lines and hence has corners where the lines intersect. The corners do not have unique normals and will represent a range of different velocity directions as shown in Figure 28. It is thus clear that almost all load states derived from the velocity directions will be at a corner and only a minimal number of velocity directions will be on the flat portions of the diagrams. Hence this might not be the best yield surface representation to use in the upper bound method. Let us now consider another system example which exploits conventional bearing capacity equations.

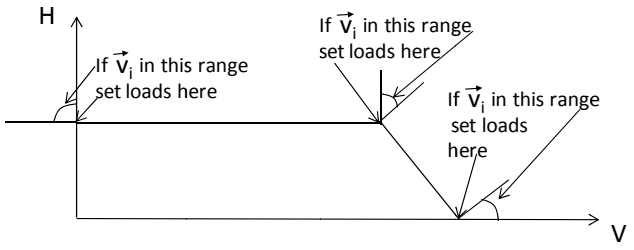

Figure 28: Corners on interaction surface result in non-unique velocity directions

Example 4

In many instances for mudmats of shallow water platforms, the lateral loads will be taken out in whole or in part by horizontal braces embedded in the soil, leg stubs or other protuberances, and/or passive pressure on peripheral skirts around mudmats. In this case it may only be necessary for the mudmats to resist the vertical loads and overturning moments imposed on the platform. Using the conventional bearing capacity equation for a strip footing with eccentricity correction (see Brinch Hansen, 1970) we can express the vertical capacity of a footing as

$$V = V_o * (1 - 2e/B) \tag{63}$$

where V_o is the bearing capacity under pure vertical load, B is the footing width parallel to the load direction, and e is the load eccentricity, $e = M/V$. We can then rearrange Equation 63 and express it as a yield function as follows

$$f(V, M) = V^2 - V_o V + 2V_o\left(\frac{M}{B}\right) = 0 \tag{64}$$

For relatively long footings we can simply multiply the strip capacity by the length, L, to get the total system capacity however for footings with $L/B < 2$ a shape factor should be applied. Figure 29 shows a non-dimensional interaction diagram of moment vs. vertical load for a single footing.

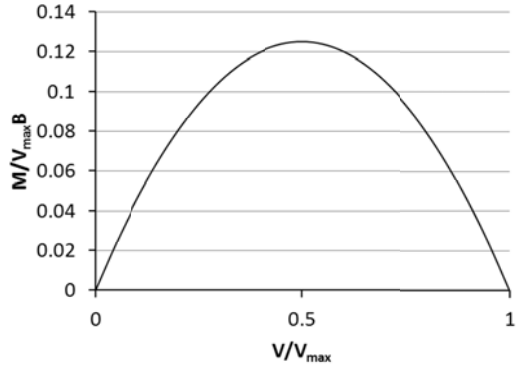

Figure 29: Single footing interaction surface with eccentricity correction

Using Equation 64 as a yield condition we can write the ratio of generalized plastic strain rates for an individual footing as

$$\frac{\dot{v}_{fi}}{\dot{m}_{fi}} = \frac{\partial f/\partial V_{fi}}{\partial f/\partial M_{fi}} = \frac{2V_{fi} - V_{ofi}}{\frac{2V_{ofi}}{B_{fi}}} \tag{65}$$

where the subscript "fi" refers to footing "i". We can then calculate the EDR for any postulated failure mechanisms for a system of footings where the system rotates about a horizontal axis located at x_o as shown in Figure 30.

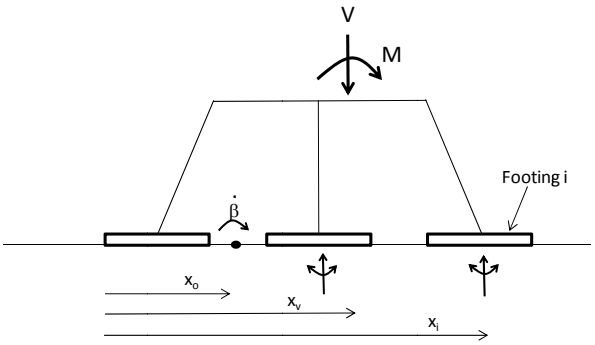

Figure 30: Schematic of failure mode for system of footings including local moment resistance

Assuming a virtual rotation rate of $\dot{\beta}$, the vertical displacement and rotation rates of footing "i" are

$$\dot{v}_{fi} = (x_0 - x_{fi})\dot{\beta} \quad \text{and} \quad \dot{m}_{fi} = \dot{\beta} \tag{66}$$

where x_{fi} is the coordinate of the footing centroid. Combining Equation 65 and 66 for each footing we can solve for V_f.

$$V_{fi} = \left(\frac{x_o - x_{fi}}{B_{fi}} + 0.5\right)V_{ofi} \tag{67}$$

Equation 67 is continuous and extends out of the range of possible values, that is for $V_{fi} > V_{ofi}$ and $V_{fi} < 0$. Hence as we did in the previous example, we must correct the values when this occurs. For example, when $V_{fi} > V_{ofi}$, it should be replaced by V_{ofi} and when $V_{fi} < 0$, it should be set to 0, assuming zero uplift capacity. Alternatively, a percentage of compression capacity could be assigned to the uplift capacity.

Knowing V_{fi} we can use the yield condition, Equation 64, to solve for M_{fi}

$$M_{fi} = \left(V_{ofi}V_{fi} - {V_{fi}}^2\right)\frac{B_{fi}}{2V_{ofi}} \tag{68}$$

The total EDR is then

$$\dot{D}_{total} = \sum_{i=1}^{n}\left[V_{fi}\left(x_o - x_{fi}\right) + M_{fi}\right]\dot{\beta} \tag{69}$$

Setting the work rate of the external loads equal to the total EDR we can solve for M

$$M = \sum_{i=1}^{n}\left[V_{fi}\left(x_o - x_{fi}\right) + M_{fi}\right] - V_{total}(x_o - x_v) \tag{70}$$

Figure 31 shows the moment-vertical load interaction diagram for a fixed two-footing system with spacing of $2B$ and eccentricity correction. For comparison, the interaction diagram for a two-footing system hinged at the connections, is also shown in the figure. It is interesting that fixing the connection against rotation only results in a very nominal improvement. The interaction diagram for a system of hinged footings where the uplift capacity is set equal to the bearing capacity is identical to the hinged case with no uplift capacity for $5.14 < V/Bs_u < 10.28$ but extends linearly upward for $V/Bs_u < 5.14$ to a value of $M/B^2s_u = 10.28$ at $V/Bs_u = 0$.

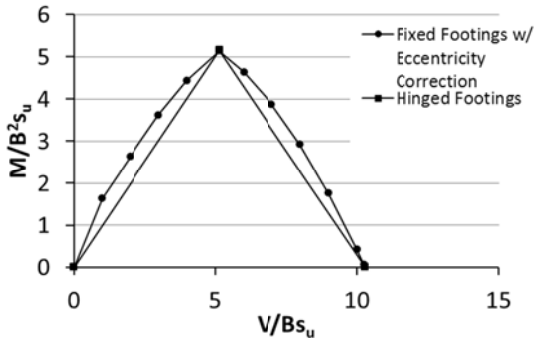

Figure 31: Footing system interaction surfaces with and without effects of local moment resistance

3.4.1 Additional Strategies

As noted in the examples above, it is straightforward to add additional footings to a system assuming they are of regular shape, aligned with the other footings, and the loading is perpendicular to one of the footing axes. For footings of different shapes, such as triangular footings, or for diagonal loading, approximations may be required. For example, it may be necessary to replace a footing of irregular geometry with an equivalent rectangular or circular footing of equal area. Vesic (1972) has also suggested shape corrections for rectangular footings loaded on a diagonal. For a system of footings loaded on a diagonal one can begin by projecting the footings on a vertical plane parallel to the load direction and solving for the system capacity assuming the footings are aligned as shown in Figure 32. It is then necessary to check for out-of-plane failure as will be discussed in more detail in the sections on pile foundations.

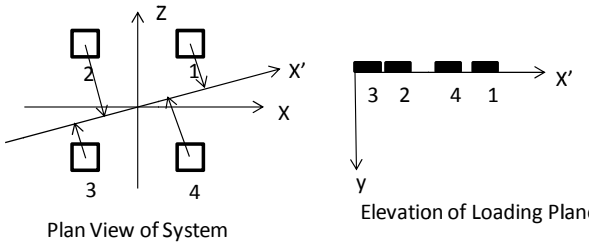

Figure 32: Off-diagonal loading with footings projected on plane of loading

In the foregoing sections on shallow foundations we have tried to identify various approaches for determining load carrying capacity of individual as well as systems of shallow foundations. We have emphasized methods of plastic limit analysis and have tried to provide some useful examples of how these methods may be applied. In the following sections we will take a similar tack for pile foundations.

4. Pile Foundations

In this part of the paper we will follow an approach similar to the one followed in the Shallow Foundations discussions. We will focus on issues uniquely related to piles. That is, where issues are the same or similar to those already discussed, we will either briefly mention them or omit them where the issue is obvious. Applications for piles vary widely over such uses as platform foundations to mooring anchors and the issues vary significantly among the various applications.

4.1 Practical issues for designing offshore pile foundations

4.1.1 Strength characterisation

Strength is clearly the most important soil parameter in foundation design and analysis. While many of the issues discussed for shallow foundations are also important for piles, a few different aspects bear specific mention.

- Is soil layering significant? Soil layering is important for all aspects of pile design but it can be particularly important in assessing end bearing capacity. Such questions as whether punch through of a hard layer over a soft layer is possible depend critically on identifying the location, strength, and thickness of interbedded layers.
- Is the soil strength affected by loading rate? This issue is particularly important as it affects the

shaft capacity of piles subjected to rapid loading such as from waves or earthquakes.

- Is the soil susceptible to creep? Piles subjected to sustained loads, particularly in uplift, may have reduced capacities due to creep. Perhaps more importantly piles subjected to uplift will tend to become unstable if they move upward significantly.
- Does the load carrying capacity of the pile exhibit softening behaviour? Very rigid piles can mobilize the peak capacity of the soil whereas piles that are very flexible may be limited to the residual capacity.
- How long will it take for full set-up to occur? This is especially important in the decision process regarding when the piles are fit for service.

4.1.2 Load characterisation

The kinds, magnitudes and locations of loads must be well understood to assess the pile requirements.

- Is the pile subjected to multi-axial loading? It is important to consider the possible load interactions imposed by moment, lateral and vertical load and torsion. What are the boundary conditions for the pile analysis? Are the piles free headed or fixed headed?
- What are the load durations? Is the pile subjected to short term loads or long term loads or both?
- Is the pile subjected to uplift loading where creep might lead to load shedding and catastrophic failure?
- Where are the loads applied? Anchor piles, for example, are less effective in resisting lateral loads if the loads are applied at the pile head.

4.1.3 Foundation geometry

The details of the pile geometry can have a strong influence on the capacity of the pile.

- Is the pile wall thickness schedule appropriate for the expected failure modes? Generally a thickened wall is needed to resist lateral loads (bending) whereas axial loading is not usually limited by stress in the pile.
- Will jacket piles be inserted in sleeves with leg stubs? Leg stubs that penetrate into the soil generally provide substantial benefits in bending resistance near the mudline.
- Are the piles long enough to develop a plastic hinge failure mode during loading or are they short enough that failure is likely to be in a fence post mode, that is kicking out at the pile tip?
- Do the piles behave individually or as a group or as a system?

The foregoing are important issues to address in deciding the critical design elements and in fact how the foundation will be analysed.

4.2 Conventional methods

4.2.1 Theory

Unlike the structure and history of shallow foundations, the conventional methods of pile analysis are not grounded in theory but are basically empirical. While they are mostly based on conceptual models, there are always empirical parameters used to carry out the design methodology. There are two distinct aspects to pile design- axial capacity and lateral performance.

The axial pile capacity is generally assumed to be the simple sum of the shaft resistance along the pile walls and the end bearing resistance at the pile tip. The basic model for pile shaft capacity in clay soils (undrained response) is

$$V_s = \pi D \int_0^L \alpha s_u(y) dy \tag{71}$$

where D is the pile diameter, L is the pile length, and α is the ratio of shear resistance mobilized at the soil-pile interface to local undrained shear strength. As such α is simply a correlation factor which is a function of a wide range of variables depending on the particular design recipe chosen. The guidelines for evaluating α generally are derived from field load tests but have also been influenced to some degree by mathematical models of an idealised installation process. Additional details of the evolution of α will be discussed in the next section. The end bearing resistance of a pile in clay is usually taken to be

$$V_{eb} = s_u N_c A \tag{72}$$

where s_u is the undrained shear strength at the pile tip and N_c is a bearing capacity factor, conceptually similar to that for shallow foundations but essentially empirical in this application. It should be mentioned however that theoretical constructions, such as cavity expansion theory as described by Bishop, et al. (1945), can be used to rationalize N_c within a reasonable range.

The soil resistance to lateral movement of the pile is usually modelled as non-linear distributed springs and the pile is modelled as an elastic beam-column. The maximum resistance of the springs per unit pile length, H, is taken to be

$$H = s_u N_p D \tag{73}$$

where s_u is the local undrained shear strength, N_p is an empirical bearing capacity factor, and D is the pile diameter. Rules for selecting appropriate N_p values have largely been derived from experiments and field tests although theoretical underpinnings for some cases have been established. Generally N_p increases with depth to account for the effect of the surface proximity until it reaches some maximum value. Guidelines for modifying the spring characteristics to account for cyclic loading effects have also been established, e.g. see Matlock (1970).

In conventional practice axial capacity is directly integrated into the foundation design. That is, the pile must have sufficient capacity to achieve a designated safety factor when compared to the design axial loads. For analysis of laterally loaded piles, the pile head loads are applied to the non-linear beam column model and the design requirements are based on limiting the stresses in the pile to allowable values. The ultimate lateral capacity of a pile is not usually a consideration. In this presentation however we will emphasize the pile's ultimate lateral capacity and argue that it provides useful insight into the foundation behaviour.

4.2.2 Applications

A very detailed history of API's axial pile capacity recommended practice is presented by Pelletier et al (1993). Only a brief summary will be provided here. It is not known exactly how the earliest offshore piles were designed for axial load although it is likely that dynamic formulae such as the Engineering News Equation (Teng, 1962), in common use at the time, were initially employed. However, by 1956, so-called static methods of analysis, as described in the "Theory" section above, were being used. These methods were pioneered for offshore applications by Bram McClelland and his co-workers and in 1962, incorporated in the standard McClelland Engineers company reports (Pelletier et al, 1993).

The first edition of API RP2A (1969) included the McClelland procedures for design of axially loaded piles. In this method the shaft resistance was taken equal to the undrained shear strength except as follows:

- For depths less than 100 feet it was limited to 1000 psf
- For depths greater than 100 feet it was limited to 1/3 of the effective overburden pressure.

The unit end bearing was specified as $9s_u$.

Over the 18 years following the publication of the first edition of RP2A there was considerable controversy over this design procedure. The uncertainties spawned a number of joint industry studies including several efforts to establish comprehensive pile load test data bases. Extensive study of these data bases was carried out by Olsen and Dennis (1982) and many different design methods were proposed. Finally a consensus evolved and in 1987 a revised method was published in the 17th edition of RP2A. The method specified that the shaft friction was taken as the undrained shear strength for soft clays but that α decreased in a systematic way as the ratio s_u/σ_v increased. It was reasoned that as the soil strength was high relative to the overburden stress, compared say to a normally consolidated clay, the soil could reduce or even partially lose its contact with the pile and hence result in a smaller percentage of adhesion. The specific method adopted is a modification of the method proposed by Randolph and Murphy (1984). The method has remained essentially the same to present day and is incorporated in the new edition of RP2GEO.

The recommendations for analysis of laterally loaded piles included in the first edition of RP2A are based on a joint industry program as documented by Matlock (1970). While a number of studies have been undertaken to generalize and validate this work, it has remained essentially unchanged to present day and is included in RP2GEO with only slight editorial comments. It is again emphasized that the proposed method of analysis involves modelling the pile-soil system as a linearly elastic beam column with non-linear soil springs resisting the lateral pile movement. As we will see the maximum resistance of the soil springs can also be used in an alternative analysis in which we assess the lateral capacity of the pile-soil system.

4.3 Plastic limit analysis – detailed mechanisms

The basic theory underlying plastic limit analysis of pile foundations is the same as that for shallow foundations. Since this has been described above, we will only consider applications in this section.

4.3.1 Applications

For the purpose here, we will consider the axial and lateral capacities independently. The mechanism associated with axial shaft failure is essentially trivial and simply involves evaluating the pile-soil bond as given by Equation 71. Because the pile tip is normally deeply embedded, disallowing any influence due to surface proximity, and the undrained soil is theoretically incompressible there is no simple mechanism associated with end bearing. Assuming

there is no softening, we simply assume the resistance is described by Equation 72 and the capacity is the sum of end and shaft capacities as discussed above. Contrary to the axial case, there are a range of possible mechanisms that can be used to investigate the various features of laterally loaded piles. Some typical examples follow below.

Example 5

Of the various mechanisms that can be defined to estimate lateral capacity we first investigate one of the simplest models. Consider a rigid pile idealised as a flat plate with width B and length L, restrained from rotation but translating laterally as shown in Figure 33. This is essentially the mechanism proposed by Reese (1958) using the limit equilibrium method. A comparison of the two solutions will be discussed later. The soil failure mechanism proposed is a triangular, rigid wedge of soil being pushed up in front of the pile. We initially assume the pile is smooth and there is a gap behind the pile so that no suction develops. We will discuss the implications of these assumptions in more detail later. The face of the soil wedge makes an angle θ with the horizontal and the soil strength is assumed to be spatially uniform.

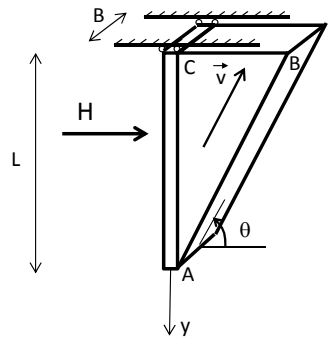

Figure 33: Schematic of idealised pile-wedge translating failure mechanism

As the pile translates to the right the soil wedge slides up the failure plane. Energy is then dissipated on the front of the wedge as it slips along the failure surface as follows

$$\dot{D}_{AB} = Area * Velocity * strength$$
$$= B\left(\frac{L}{\sin\theta}\right) * \frac{v_o}{\cos\theta} * s_u = \frac{BLs_u v_o}{\sin\theta\cos\theta} \qquad (74)$$

The EDR on the two sides of the soil wedge is then

$$\dot{D}_{ABC-S} = \frac{L^2 s_u v_0}{\sin\theta} \qquad (75)$$

The work rate of the lateral force is simply $= Hv_o$ and the work rate in lifting the soil wedge is

$$\dot{W}_\gamma = Volume * \gamma' * v_v = -\frac{1}{2}L^2 B\gamma' v_o \qquad (76)$$

where γ' is the effective unit weight and v_v is the vertical velocity of the wedge. The upper bound equation is then

$$Hv_o - \frac{1}{2}\gamma' L^2 B v_o = \frac{BLs_u v_o}{\sin\theta\cos\theta} + \frac{L^2 s_u v_o}{\sin\theta} \qquad (77)$$

Thus the lateral capacity of the translating pile is then

$$H = \frac{BLs_u}{\sin\theta\cos\theta} + \frac{L^2 s_u}{\sin\theta} + \frac{1}{2}\gamma' L^2 B \qquad (78)$$

The solution is then minimized with respect to θ to find the best solution. Note that the work done in lifting the soil weight is negative since the mechanism is working against gravity. Further the contribution of the soil weight to capacity is, in effect, the average of the effective overburden pressure over the pile length times the vertical cross sectional area of the pile and is independent of θ. Such independence results because the soil is incompressible and any net displaced volume in the soil must be displaced upward to the free surface in any admissible mechanism. Note that for $B \gg L$ the contribution of the sides becomes insignificant and the solution approaches the Rankine solution for passive pressure on a wall with a critical θ value of 45°.

An obvious feature of this mechanism is that the average pressure continues to increase indefinitely as the pile length increases. Clearly at some depth the soil will not be displaced upward but will flow around the pile. At that depth and below, the proximity of the free surface will have no effect on the resistance. Consider an infinitely thin plate deeply embedded and loaded normal to its surface so that soil flow around the plate occurs. A characteristics solution can be found for this case as shown in Figure 34.

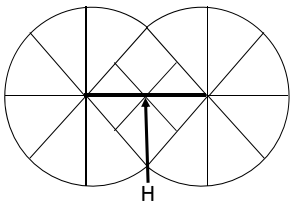

Figure 34: Characteristic solution of deeply embedded flat plate under normal load

The net pressure developed on the plate over a unit length in this case is

$$\frac{H}{(1)B} = N_p s_u = (2+3\pi)s_u = 11.42 s_u \tag{79}$$

Now we will modify the mechanism shown in Figure 33 to include two zones. The wedge of the previous solution is assumed to act above the depth, L_1 and flow around occurs below the depth L_1 as shown in Figure 35.

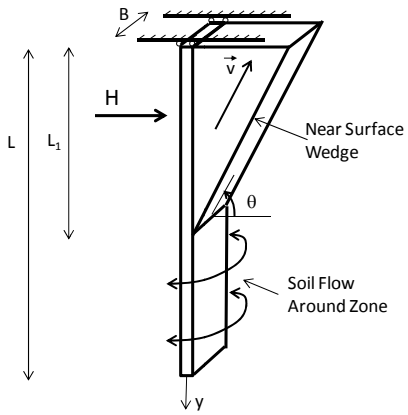

Figure 35: Schematic of idealised pile-wedge failure with flow-around at depth

We then replace L in Equation 78 with L_1 and add a term to account for the dissipation below L_1 as shown here

$$Hv_o = \frac{BL_1 s_u v_o}{\sin\theta\cos\theta} + \frac{{L_1}^2 s_u v_o}{\sin\theta} + N_p(L-L_1)Bs_u v_o + \frac{1}{2}\gamma' {L_1}^2 B v_o \tag{80}$$

The solution can then be written in a non-dimensional form

$$\frac{H}{BLs_u} = \frac{L_1/L}{\sin\theta\cos\theta} + \frac{\left({L_1}^2/L^2\right)\left(\frac{L}{B}\right)}{\sin\theta} + N_p(1-L_1/L) + \frac{1}{2}\left(\frac{\gamma' B}{s_u}\right)\left(\frac{{L_1}^2}{L^2}\right)\left(\frac{L}{B}\right) \tag{81}$$

In this model both L_1 and θ are minimization variables. It should be noted that this model is no longer a rigorous upper bound since we have not explicitly accounted for details of the wedge-flow around transition. While this solution has reasonable appeal it is clearly an approximation. N_p represents only the contribution of the soil strength to resistance and thus to estimate N_p we set the unit weight of the soil to zero. To find N_p above the flow-around zone we incrementally increase L and compute the minimum H for each L value. We find that the optimum value of both θ and L_1 change as the pile length increases. We make the assumption that the increase in lateral capacity ΔH is totally attributed to the load on the added pile increment ΔL, that is the load distribution on the pile above the increment does not change with the added pile increment so that

$$\Delta H = N_p \Delta L B s_u \tag{82}$$

or

$$N_p = \frac{\Delta H}{\Delta L B s_u} \tag{83}$$

Figure 36 shows the results of estimating N_p as a function of depth using Equation 83. On this plot we have also included a plot of the right hand side of Equation 83 for a case with finite unit weight, specifically the parameter $\gamma' B/s_u = 1$. For the weightless case the flow-around zone begins at a depth of $L/B = 3.94$. N_p can be approximated by the linear function $2 + 2.4\,L/B$. For the finite soil weight case, the soil weight increases the pressure on the pile and once the combined pressure equals $11.42 s_u$, flow-around is initiated. In this case i.e. $\gamma' B/s_u = 1$, it begins at $L/B = 2.73$.

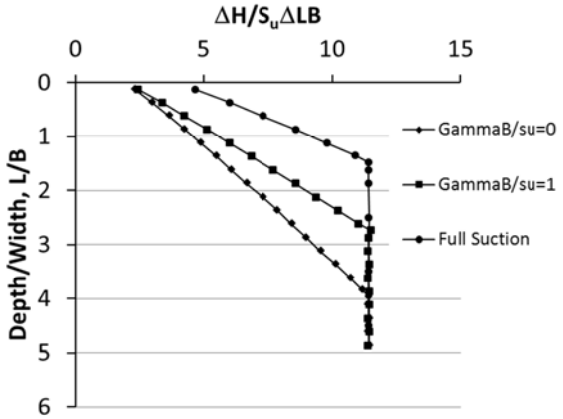

Figure 36: Plot of inferred N_p vs. depth values from wedge model

Now if it is assumed that there is no gap at the back of the pile, an active wedge will form which will be identical to the passive wedge and for any wedge depth will double the resistance due to dissipation over that part of the mechanism. Obviously this will result in reaching the flow around pressure at a shallower depth. However, the negative work done in lifting the passive soil wedge will be exactly compensated by the positive work done by the active soil wedge and hence the soil weight will have no net effect on the solution. Again we have plotted the right hand side of Equation 83 for this case in Figure 36 showing the flow-around transition occurs at $L/B = 1.47$.

In the preceding discussion we considered a pile rigidly translating through the soil such as might occur if the pile head is fixed against rotation. Of course mechanisms involving pile rotation are also possible and are discussed in the following example.

Example 6

Figure 37 shows possible mechanisms with pile rotation. Figure 37(a) shows a free headed pile rotating rigidly in the so-called fence post failure mode; Figure 37(b) shows a pile yielding (forming a plastic hinge) at the mudline and rotating below that point; and Figure 37(c) shows a pile with two plastic hinges failing in a shear type mode.

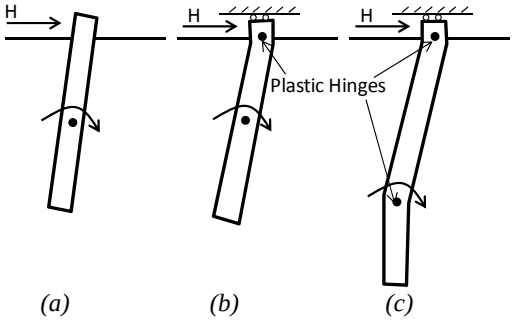

Figure 37: Schematics of idealised rotation mechanisms (a) free-head pile (b) pile with plastic hinge at mudline (c) pile with two plastic hinges

Pile rotation can be accommodated by the wedge mechanism discussed previously by allowing the wedge to deform as well as translate as shown in Figure 38. In this mechanism the pile is assumed to rotate rigidly about O, the soil below L_1 flows around the pile, and the soil above L_1 moves in a wedge that is both shearing and translating. Slight modifications of this mechanism, say to account for pile yielding, can be made to model the other mechanisms in Figure 37 and will be discussed in a later section.

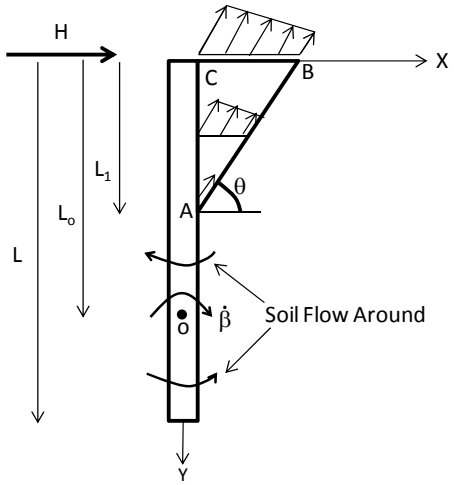

Figure 38: Schematic of soil wedge to accommodate pile rotation

Figure 38 shows a detailed velocity field for the wedge. The soil in the wedge is assumed to move parallel to the boundary AB and to conform to the pile motion along AC. Assuming the virtual velocity in the horizontal direction at the pile top is v_o, the rotation rate, $\dot{\beta}$, is then equal to v_o/L_o. Further assume that the resultant velocity varies linearly with x from the pile interface to the wedge face. At any point along the pile-wedge interface, the x velocity is

$$v_x = v_o\left(1 - \frac{y}{L_o}\right) \tag{84}$$

To accommodate the pile motion, v_x at A and consequently all along AB is then

$$v_x = v_o\left(1 - \frac{L_1}{L_o}\right) \tag{85}$$

It then follows that, within the wedge

$$v_y = -v_x \tan\theta \tag{86}$$

We can then derive a general velocity field within the wedge as

$$v_x = v_o\left(1 - \frac{y}{L_o} - \frac{\tan\theta}{L_o}x\right) \tag{87}$$

and

$$v_y = -v_o\left(1 - \frac{y}{L_o} - \frac{\tan\theta}{L_o}x\right)\tan\theta \tag{88}$$

The relevant strain rates are then

$$\dot{\varepsilon}_x = \frac{\partial v_x}{\partial x} = -\frac{v_o\tan\theta}{L_o} \tag{89}$$

$$\dot{\varepsilon}_y = \frac{\partial v_y}{\partial y} = \frac{v_o\tan\theta}{L_o} \tag{90}$$

and

$$\dot{\varepsilon}_{xy} = \frac{1}{2}\left(\frac{\partial v_x}{\partial y} + \frac{\partial v_y}{\partial x}\right) = \frac{v_o}{2L_o}(\tan^2\theta - 1) \tag{91}$$

After some simplification we find that

$$|\varepsilon_1|_{max} = \frac{v_o}{2L_o\cos^2\theta} \tag{92}$$

which is a constant over the wedge volume. The total EDR within the wedge is then

$$\dot{D}_{ABC} = \frac{s_u {L_1}^2 B v_o}{2L_o\cos\theta\sin\theta} \tag{93}$$

The EDR on the slip surface is equal to

$$\dot{D}_{AB-B} = v_{result} * s_u * Area$$
$$= \frac{s_u L_1 B v_o}{\cos\theta \sin\theta}\left(1 - \frac{L_1}{L_o}\right) \quad (94)$$

The EDR on the two sides of the deforming wedge is found by integrating the relative slip velocity over the areas which gives

$$\dot{D}_{ABC-S} = \frac{s_u v_o}{\sin\theta}\left({L_1}^2 - \frac{2{L_1}^3}{3L_o}\right) \quad (95)$$

Below the wedge it is assumed that the soil's unit resistance is simply equal to $N_p s_u$ and the local EDR is then $N_p s_u B v_x$ which must be integrated over the length from L_1 to L. The total EDR for $L_1 < L_o < L$ is then

$$D_{L_1-L} = \int_{y=L_1}^{L_o} v_o\left(1 - \frac{y}{L_o}\right) N_p B s_u dy + \int_{y=L_o}^{L} v_o\left(\frac{y}{L_o} - 1\right) N_p B s_u dy \quad (96)$$

Note that the velocity changes directions at L_o but so does the resistance, so the expressions change. After some simplifications the EDR below L_1 is found to be

$$\dot{D}_{L_1-L} = v_o N_p B s_u\left(L_o - L_1 - L + \frac{{L_1}^2 + L^2}{2L_o}\right) \quad (97)$$

Using a similar approach for $L_o > L$ the EDR is

$$\dot{D}_{L_1-L} = v_o N_p B s_u\left(L - L_1 - \frac{L^2 - {L_1}^2}{2L_o}\right) \quad (98)$$

The work rate of the external forces is then set equal to the sum of the EDRs for this mechanism. The capacity is then minimized with respect to θ, L_1, and L_o to find the critical value. Figure 39 shows a plot of the normalized capacity H/LBs_u for the rotating pile and the rigidly translating pile demonstrating the significant difference in the two. For $B \gg L$ the rotating pile (or wall) solution is exactly one-half of the Rankine solution as expected.

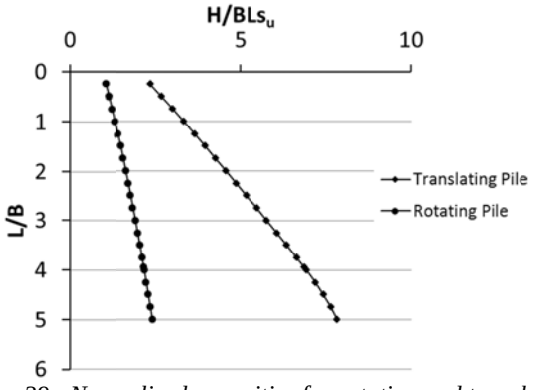

Figure 39: Normalized capacities for rotating and translating piles

4.3.2 Additional Strategies

In the foregoing examples the pile was idealised as a smooth, rigid, flat plate in a uniform strength clay. Clearly there are situations where more general descriptions are desired. For example it is straight forward to include varying degrees of pile roughness by adding another dissipation term equal, to α times the soil's vertical velocity relative to the pile times vertical cross section area of the pile in contact with the wedge times s_u. Non-homogeneous soil strength can also be incorporated in the solution by including the soil strength as a function of depth in the integrations of EDR over surfaces and volumes. Finally in offshore applications, pipe piles are normally employed and thus a circular geometry is more realistic as will be discussed below.

One solution that has been particularly useful in this regard is the characteristics solution developed by Randolph and Houlsby (1984) for a deeply embedded circular pipe translating perpendicular to its axis. Solutions using characteristic nets were derived in that paper for pile-soil interfaces varying between smooth and rough. It is interesting that the authors developed the solution without formal integration of the characteristic equations but by simply reasoning based on the problem symmetry, boundary conditions, and well known properties of the characteristic curves (Randolph Personal Communication). The force per unit length was found to range from $(6+\pi)cd$ for a smooth pile to $\left(4\sqrt{2}+2\pi\right)cd$ for a rough pile where *c* is undrained shear strength and *d* is pile diameter. They suggested a linear function of the adhesion factor, specifically $(9+3\alpha)$ as a good empirical fit to their solutions.

Murff and Hamilton (1993) used the Randolph and Houlsby solution (1984) for the deeply embedded part of the pile along with a modified wedge mechanism to accommodate a circular pile for shallow

depths. Their proposed failure mechanism is shown in Figure 40.

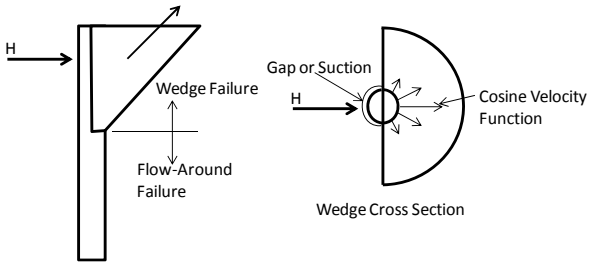

Figure 40: Murff-Hamilton failure mechanism for a pipe pile with circular cross section

They proposed an intuitive mechanism where the soil wedge has a radial velocity of

$$v_r = v_o \left(\frac{R}{r}\right)^{\alpha} \left(1 - \frac{z}{z_o/c}\right) \cos\theta \tag{99}$$

where R = pile radius; r, z, and θ are cylindrical coordinates; z_o = wedge depth, (z_o/c) = depth to centre of rotation (similar to L_o in the rotating pile example above) and α = exponent. In this velocity field $v_\theta = 0$ so that resultant velocities are strictly in the $r - z$ planes. The radial velocity is a maximum at $\theta = 0$, the very front of the pile, and decays to zero at $\theta = \pm 90°$ owing to the cosine function. Imposing the incompressibility condition on the velocity field gives

$$\dot{\varepsilon}_{rr} + \dot{\varepsilon}_\theta + \dot{\varepsilon}_z = \frac{\partial v_r}{\partial r} + \frac{v_r}{r} + \frac{\partial v_z}{\partial z} = 0 \tag{100}$$

which, along with Equation 99 and the boundary conditions, provides the necessary equations to define the complete velocity field. This in turn allows one to calculate the strain rates and hence the EDR in the wedge mechanism. Below the wedge is considered to be a flow-around zone which is treated in a similar manner as the examples above. These calculations are detailed by Murff and Hamilton (1993). Thus the problem can be set up in a similar manner to the rotating pile problem described above and solutions obtained by optimizing the upper bound solution with respect to α, c, z_o, and r_o, the latter being the radial extent of the wedge at $\theta = 0$. The solution has been exercised for a range of conditions to determine N_p vs. depth profiles as we have previously done. For example, such profiles are developed for a range of interface adhesion values and typical soil strength profiles.

4.4 Generalized Plastic Limit Analysis- Macro-Mechanisms

The basic principles of generalized plastic limit analysis discussed above are applicable to pile problems of interest and so we again will consider only applications in this section.

4.4.1 Applications

As discussed previously, the macro-mechanism perspective is to look at problems in terms of forces and displacements rather than specific soil velocity fields with their accompanying detailed stress and strain fields. The axial capacity mechanisms alone are straightforward and need little discussion although some discussion of how they interact with lateral mechanisms will be considered below. The lateral mechanisms require a little more attention.

In the lateral mechanisms we consider a defined soil resistance distribution along the pile which is a result of the soil failure mechanism but does not include it explicitly. This force distribution may come from empirical methods such as the Matlock (1970) definition of $P_{ultimate}$, numerical studies such as finite element analysis, or be inferred from limit analysis solutions as was done in the previous section where N_p was estimated. These ideas can again best be explained by means of examples.

Example 7

Consider a rigid pile, loaded laterally at the top and free to rotate as shown in Figure 41. For the purposes of illustration we consider a simple case where the soil resistance on the pile, R, is constant with depth. The failure mechanism considered is rotation of the pile about a horizontal axis at depth L_o as shown in Figure 41.

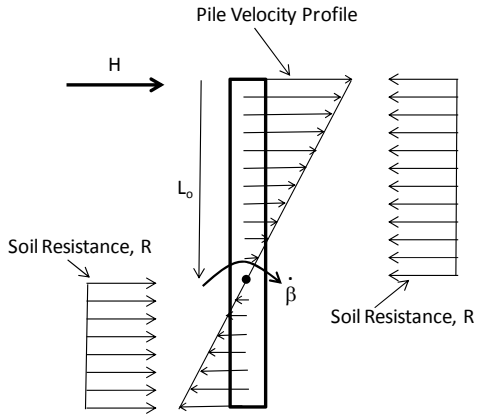

Figure 41: Schematic of a rigid pile, loaded at the top and free to rotate

The dissipation rate is then

$$\dot{D} = \int_0^{L_p} R * v(y) * dy \tag{101}$$

Note that both velocity and resistance change directions (signs) below L_o so that

$$\dot{D} = \int_0^{L_o} R * (L_o - y)\dot{\beta} * dy + \int_{L_o}^{L} R * (y - L_o)\dot{\beta} * dy \quad (102)$$

The external work rate $= HL_o\dot{\beta}$ so setting these expressions equal and simplifying gives

$$H = R\left(L_o + \frac{L^2}{2L_o} - L\right) \quad (103)$$

Minimizing H with respect to L_o then gives $L_o = L/\sqrt{2}$. Substituting into Equation 103 gives $H = RL(\sqrt{2} - 1)$. While this is a trivial solution, the approach is the same as for more realistic resistance and pile descriptions as discussed below

The piles for steel piled jackets are effectively fixed against rotation at the mudline and sufficiently deep that the pile will not "fence post". As a result of these conditions a possible failure mode will consist of formation of two plastic hinges, one at the mudline and the other at some depth below the mudline resulting in a shear type failure mode as shown in Figure 37(c) above. Further a linearly increasing soil resistance, say $R_o + R_1 y$, is a more realistic model than a constant resistance. At each plastic hinge the pile develops a plastic moment resistance of *M*. These facts lead to an EDR in the soil of

$$\dot{D}_s = \int_0^{L_o} (R_o + R_1 y) * \left(1 - \frac{y}{L_o}\right) v_o dy \quad (104)$$

and an EDR due to the plastic moments of $2M_p v_o/L_o$. The external work rate is simply Hv_o. Setting the work rate equal to the sum of the dissipation rates, cancelling v_o, and solving for H gives

$$H = \int_0^{L_o} (R_o + R_1 y) * \left(1 - \frac{y}{L_o}\right) dy + \frac{2M_p}{L_o} \quad (105)$$

Note that we could further generalize this expression by including any soil resistance function in the integral. Further a free headed pile that forms a plastic hinge below the mudline, such as might be employed as an anchor, can be modelled by changing $2M_p$ to M_p.

Equation 105 can be integrated analytically but it is a simple matter to set up numerical integration where the resistance function can be changed easily. Finding the optimum for the general case can be difficult but optimization routines such as the Solver Function© makes the process quite simple even for numerical integration. Closed form solutions for the ideal cases, $R_1 = 0$ and $R_o = 0$, can be found easily using the standard approach as follows

$$R_1 = 0:\ L_o = 2\sqrt{\frac{M_p}{R_o}} \ \Rightarrow\ H = 2\sqrt{M_p R_o} \quad (106)$$

$$R_o = 0:\ L_o = \sqrt[3]{\frac{6M_p}{R_1}} \ \Rightarrow\ H = \sqrt[3]{\frac{9{M_p}^2 R_1}{2}} \quad (107)$$

These solutions provide useful "back of the envelope" equations that can provide quick insight into a problem.

An additional, related problem of interest is the capacity of a laterally loaded pile where an anchor line is attached deeply embedded in the soil so that proximity to the mudline has no influence. Assuming a uniform soil resistance over the section of pile in question and a three hinge mechanism as shown in Figure 42, the problem is set up in a similar manner to that above.

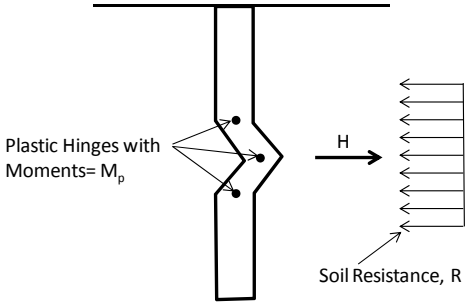

Figure 42: Schematic of a three-hinge failure mechanism for a deeply embedded anchor line attachment point

The ultimate capacity of the pile anchor is then

$$R_1 = 0:\ L_o = 2\sqrt{\frac{M_p}{R_o}} \ \Rightarrow\ H = 4\sqrt{M_p R_o} \quad (108)$$

As mentioned above it is relatively simple to set up numerical solutions that have considerably more complexity on a spreadsheet.

Example 8

Having explored the ultimate lateral capacity of single piles to some degree, it is of interest to investigate the capacity of pile systems. Consider a simple 4-pile example. As shown in Figure 43(a), the pile images are projected onto a vertical plane aligned with the lateral load. The planar capacity is then determined for the projected systems as characterised in Figure 43(b). The failure mechanism is assumed to be a virtual rotation, $\dot{\beta}$, of the system about a horizontal axis through the point x_o, y_o. The piles are

deeply embedded and fixed to the structure which is assumed rigid so they will form plastic hinges at the connection points and at a depth L_o, as yet unknown.

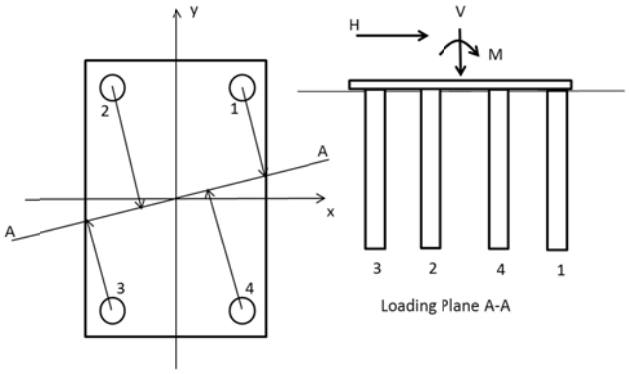

(a)

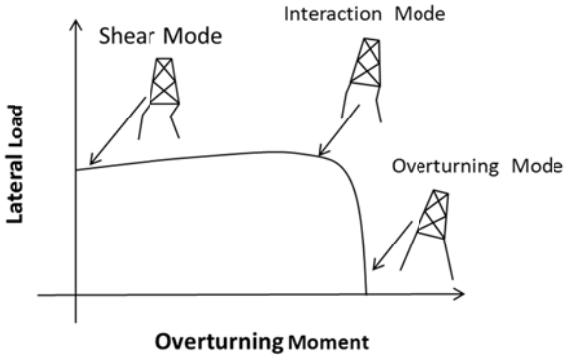

(b)

Figure 43: Schematic of a four pile system (a) Pile images projected on a vertical plane (b) Capacity of the planar system

Figure 44 shows a generic pile in the system. The velocity at the pile head is resolved into components parallel and perpendicular to the pile's axis, v_{yi} and v_{xi}, respectively. The rotation rate of the upper section of the pile about L_o is then $y_o\dot{\beta}/L_o$ whereas the rotation rate of the base of the structure is simply $\dot{\beta}$. The plastic hinge at the pile head then undergoes a net rotation with respect to the structure of $\dot{\beta}(1 - y_o/L_o)$ and the hinge at L_o rotates at $y_o\dot{\beta}/L_o$.

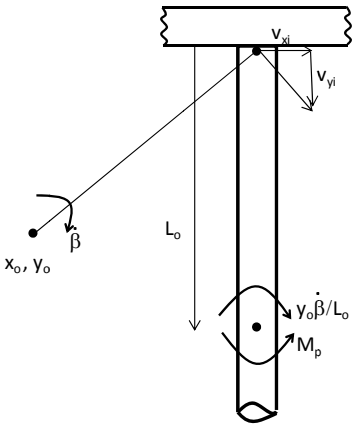

Figure 44: Schematic of a generic pile in the four pile system

These values allow the calculation of the EDR of the plastic moments of

$$\dot{D}_M = M_p\left(1 - \frac{y_o}{L_o}\right)\dot{\beta} + M_p\left(\frac{y_o}{L_o}\right)\dot{\beta} \tag{109}$$

The lateral velocity of the pile above L_o is given as

$$v_{xi} = y_o\left(1 - \frac{y_i}{L_o}\right)\dot{\beta} \tag{110}$$

and the axial velocity at the pile head is

$$v_{yi} = (x_i - x_o)\dot{\beta} \tag{111}$$

These results provide the necessary input to calculate the EDR. The external work rate is

$$\dot{W} = H(y_o + y_h)\dot{\beta} + V(x_w - x_o)\dot{\beta} \tag{112}$$

where H and V are the horizontal and vertical global loads on the system. We can then apply the upper bound method to solve for horizontal capacity

$$H = \frac{\sum_1^4 y_o \int_0^{L_o}\left|1 - \frac{y_i}{L_o}\right| R(y_i)dy}{y_o + y_h} + \frac{\sum_1^4 (x_i - x_o)Q + 4M_p\left(\left|1 - \frac{y_o}{L_o}\right| + \left|\frac{y_o}{L_o}\right|\right)}{y_o + y_h} - \frac{V(x_w - x_o)}{y_o + y_h} \tag{113}$$

where Q = axial pile capacity. Equation 113 is then minimized with respect to x_o, y_o, and L_o. It has been found that L_o determined for an individual pile remains relatively constant for the group and the results are very insensitive to it so L_o can be determined prior to the system optimization.

A simple example of the four-pile system is described in Table 1.

Table 1: Parameters for analysis of four-pile foundation

Parameter	Value
V/Q	0 and 2
M/QB	0.10
RB/Q	0.40
x_1/B	0.50
z_1/B	0.50

An interaction diagram of horizontal load vs. overturning moment is shown in Figure 45. There are three zones of interest. At small moments, say loads near the mudline, the failure is a shear mechanism characterised by lateral translation and double hinges in the piles. At relatively small horizontal loads

the failure is overturning characterised primarily by axial failure of the piles. A region between is a zone of horizontal load-moment interaction where both bending and axial load in the piles is apparent. Figure 45 also shows the effects of a vertical load such as the structure weight which reduces the moment capacity but not the shear capacity. This of course presumes that the plastic moments in the piles are not significantly affected by the axial loads.

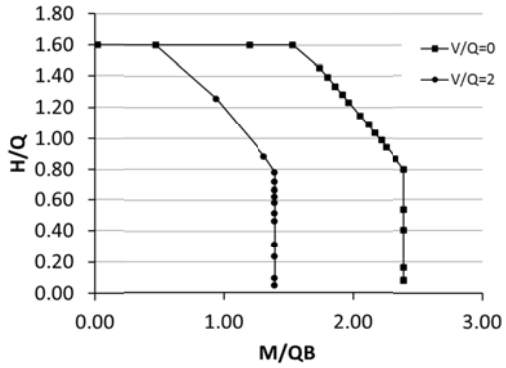

Figure 45: Interaction diagram of lateral load vs. overturning moment for a four pile system

In this analysis the failure is assumed to be in the plane containing the resultant horizontal load. This overly constrains the system and does not admit the possibility of an out-of-plane failure. It would be possible to include the direction of failure as an additional parameter in the optimization procedure however we prefer an alternate strategy which gives the analyst a little more control over the analysis. The alternate procedure is shown in Figure 46, an interaction diagram of *x* and *y* forces for a fixed load height of $3B$ for a rectangular base of $Bx2B$.

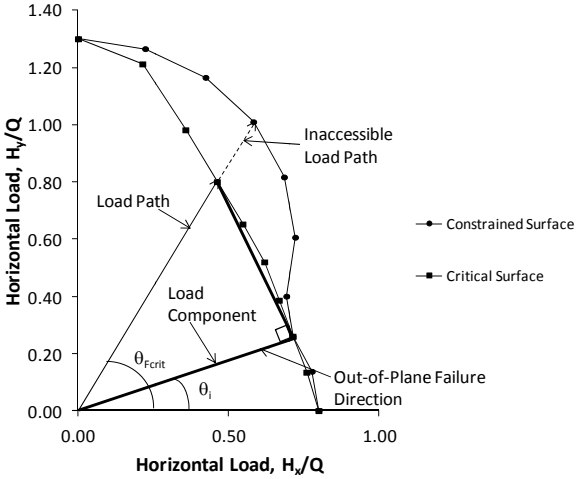

Figure 46: Interaction diagram of lateral forces in x and y directions with base dimensions B x 2B

The rectangular base accentuates the effect of constraining the failure direction. Note the significant bulge in the interaction diagram. In this region the foundation can fail in an out-of-plane direction as demonstrated in Figure 46. As shown in the plot the load cannot actually reach the constrained failure surface on this path since a component of the load will reach the failure at another location first. In this analysis, each possible load path is tested against all points on the constrained failure surface to determine at what point a component of that load will first reach the surface. Thus the critical magnitude of the load along the load path is given as

$$F_{crit} = Min\left[\frac{F_i}{\cos\theta_{F_{crit}} - \theta_i}\right] \tag{114}$$

where F_{crit} is the critical load value at the load angle $\theta_{F_{crit}}$ and F_i represents all possible load values at the respective angles θ_i. The critical or governing yield surface is the result of analysing possible load paths from zero to 90°. The reduced interaction surface in Figure 46 has been corrected to include the possibility of out-of-plane failure.

4.4.2Additional Strategies

In the foregoing, the examples were intentionally simple to demonstrate the concepts without getting bogged down in too many details. It is important to point out however that significantly more realism can be included without the analysis becoming too onerous. Of course at some level of effort a more rigorous analysis such as finite elements may be called for and in fact at least some such is recommended to calibrate the simpler methods. In the following we include a few ideas where added realism is not too burdensome.

The region of a pile involved with the lateral failure mechanism is also subjected to axial loads or shear along the pile. This can result in a reduction in lateral capacity due to the interaction of normal and shear stresses on the pile face. Aubeny, et al. (2002) used results from finite element analysis to characterise this interaction and include it as a distributed yield surface (over the pile surface) in an upper bound model. This concept has been shown to be particularly useful in the analysis of large diameter piles such as suction caissons subjected to inclined loads.

Additional modifications for the pile system can also add realism to the analysis. Examples include pile batter, variable wall thickness, and moment-axial load interaction. Pile batter can be accommodated by resolving the velocities parallel and perpendicular to the pile axes. Pile wall thickness profiles can be used in the search for the depth of the second plastic moment. The plastic moment can also be made a

function of the axial load by including the axial load-plastic moment interaction relationship as a yield surface in the model so that rotation rate and axial velocity are generalized strain rates as discussed by Murff (1987). Of course, it is also straightforward to include additional piles in the model.

A recent innovative shallow foundation concept uses short "pin" piles in the corners of a mud mat to provide additional support and reduce the mud mat area for more efficient offshore handling and installation. The above mentioned pile system model can be modified easily by replacing the lower plastic moment mechanism with a rigid pile that kicks out below the pile rotation depth.

The ideas above are just a few of the modifications that can be incorporated in models previously discussed to provide better insight into foundation behaviour. This emphasizes the significant role that innovation plays in constructing mechanisms. Plastic limit analysis provides a convenient set of rules for consistently analysing surprisingly complex models.

5. Plastic Limit Analysis and the Limit Equilibrium Method

It is sometimes argued that soils do not obey the associated flow rule and hence PLA methods do not reflect real behaviour. Further the upper bound method gives results that are unconservative in most applications and hence limit equilibrium methods that focus on satisfying statics are to be preferred. It might therefore be useful to put in perspective the concepts of plastic limit analysis as related to the limit equilibrium method. First it should be pointed out that the collapse load estimate is usually not very sensitive to the assumption of associated flow. As pointed out by Davis (1968) this is true even for frictional materials where dilation is known to be significantly over predicted. In a sense we can think of upper bound solutions as getting as close to equilibrium as possible for the proposed failure mechanism. The early limit equilibrium solutions by Coulomb, Rankine, and others were conceived well before the principles of plasticity were deduced. In these models failure mechanisms were constructed and an attempt made to satisfy equilibrium and the failure conditions along the hypothesized failure surfaces. As pointed out by Murff and Miller (1978) the limit equilibrium methods borrow from both the upper and lower bound ideas. They resemble upper bounds in that mechanisms are proposed and they resemble lower bounds in the attempt to satisfy global equilibrium and yield. However, they do not include checks to establish that the mechanisms are kinematically admissible nor that stress conditions within the mechanisms are statically possible.

In most classic solutions such as Coulomb's and Rankine's, the solutions are in fact admissible while the process of imposing global equilibrium and yield is actually equivalent to formulating the upper bound equation. These solutions generally do not rigorously satisfy equilibrium and yield in the small. As such they are actually valid upper bound solutions as can be shown by comparing the solutions with an upper bound formulation. As an example consider the solution for a laterally loaded pile using the wedge mechanism as proposed by Reese (1958) and shown in Figure 47.

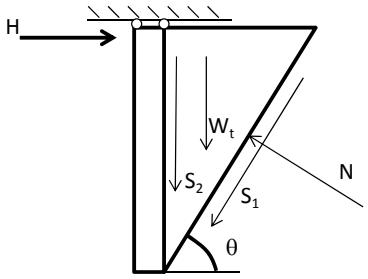

Figure 47: Schematic of limit equilibrium solution using the wedge mechanism

The solution proposed was to sum shear and normal forces acting on the various faces of the wedge in the vertical and horizontal directions and to solve the two resulting equations simultaneously. This model includes the normal force on the wedge face. It is unnecessary to include this force in the upper bound solution as it does no work nor dissipates energy in the deforming mechanism and a single, simpler equation results from the virtual work formulation. The upper bound solution as given in Equation 78 above turns out to be identical to Reese's limit equilibrium solution. Both solutions require minimization with respect to the wedge angle to get the best solution i.e. the one closest to equilibrium. This best solution while being a reasonable approximation is not the true mechanism and clearly does not satisfy equilibrium and yield. This is most evident by the fact that the wedge failure surfaces do not intersect free surfaces at 45°. Thus where the limit equilibrium method employs a kinematically admissible mechanism it produces the same result as the upper bound solution for that mechanism. The upper bound method however is simpler in its formulation as shown here and more adaptable to complex conditions. For example in contrast to the limit equilibrium method the upper bound approach easily incorporates deforming regions in the mechanism and is

much more adaptable to non-homogeneous strength profiles.

In some applications the ideas of the limit equilibrium method have been extended to non-standard problems where mechanisms are constructed of lines simulating "intuitive" failure surfaces, for example seeking to exploit weak layers. Such mechanisms may or may not be admissible ones and hence can lead to rather arbitrary results. To illustrate this point Figure 48 shows examples of some solutions that seem reasonable but are not in fact admissible.

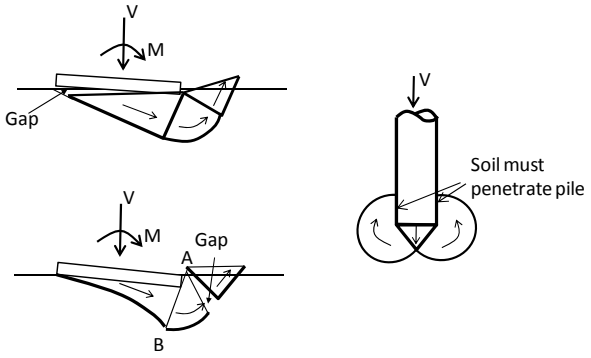

Figure 48: Schematic showing example inadmissible failure mechanisms

Figure 48(a) attempts to include the effects of moment loading in a planar mechanism. Again this implies a gap opening on the left side which is inadmissible. To include moment effects the mechanism must provide for rotation such that the moment does work and the soil deformation does not include separations.

Figure 48(b) includes rotation of the system about a horizontal axis below the footing. As such the velocity of the right corner of the footing, A, is greater than the points below it, say at B. Thus if the wedge on the right side is rigid, a gap will form as shown. The mechanism can be made admissible by allowing the wedge to deform.

Figure 48(c) shows a failure mechanism at a deeply embedded pile tip. In this case advancing the pile tip requires the change in volume to be accommodated in the mechanism. Since the consistent soil model is incompressible (for clay) or dilatant (for sand) the volume change cannot be accommodated unless the mechanism intersects the soil surface. This will generally give a very poor result. For deep embeddments, the conventional PLA methods cannot be used and one must resort to cavity expansion solutions such as proposed by Bishop, et al. (1945) in which the collapse pressure is a function of the elastic stiffness and the soil shear strength.

6. Closing Comments

It has been the intention of this paper to use simple examples to shine a light on the robust generality of PLA methods and to hint at their ability to obtain approximate and useful solutions to complex problems. It is argued that, properly applied, these methods achieve the same thing that more traditional limit equilibrium methods achieve when correctly formulated. Thus the argument here is by no means to abandon traditional methods but to use PLA methods to build on the limit equilibrium techniques and add to their generality and consistency.

In cases where more rigorous methods such as finite element methods are to be used, PLA methods can play an important role. Preliminary studies can be used effectively to design the finite element studies and they can be used very effectively to supplement the finite element studies as they are being carried out.

PLA methods are thus important tools in the engineer's arsenal and with a little practice can be exploited to add surprising insight into even complex problems- and insight is what computation is all about.

7. Acknowledgements

I want to express my sincere appreciation to the ISSMGE for inviting me to give the inaugural Bramlette McClelland Lecture. Bram was a true visionary and rightly considered the Father of Offshore Geotechnical Engineering. He has been a role model for me since I began my career in this field.

I would first like to acknowledge the organizations I have been affiliated with over the years that have profoundly influenced my life: The US Military Academy at West Point, the US Army, Texas A&M University, and Exxon Production Research Company. I have learned valuable career and life lessons during my tenures with each and I am greatly indebted to them.

My wife of 49 years and partner, Jeanie, has supported me every step of the way, often cheerfully sacrificing her own pursuits to allow me to follow mine. My sons Jim and Roger have always been a source of support and pride.

There are so many colleagues that have helped me in so many ways that I hesitate to name names but I feel I must acknowledge a few that have been so important. Alan Young, my lab partner in my first soil mechanics course has been a friend and mentor since our days together at Texas A&M; Terry Miller, a

high school classmate, who later became a valued colleague and tutored me in the challenging field of plasticity; Mark Randolph has taught me so much and has frequently gone out of his way to publicly recognize my work; Charles Aubeny who I collaborated with at Texas A&M and who contributed so much to my education; my friends at BP Ed Clukey and Philippe Jeanjean. Ed has been a colleague for many years starting with our days together at Exxon; Philippe was one of my first students. Both have gone on to highly successful careers and have kept me engaged in interesting and rewarding projects since my retirement from Exxon. And there are many, many more. Thank you.

Finally I want to acknowledge Jill Rivette, P.E. who is among other things an expert in the vagaries of Word, and who has hammered my very, very rough drafts of this paper into a thing of beauty. How can I ever repay you?

8. References

American Petroleum Institute. (1969-2000). *Recommended Practice for Planning Designing, and Constructing Fixed Offshore Platforms- Working Stress Design RP2A*. Editions 1- 21. Washington DC.

American Petroleum Institute and International Standardization Organization. (2011) ANSI/API Specification *RP2GEO, Geotechnical and Foundation Design Considerations for Offshore Structures*.

Aubeny CP, Han SW and Murff JD. (2003) Inclined load capacity of suction caissons. *Int. Jrnl. Numerical and Analytical Meth. in Geomechanics* , Vol. 27, 1235-1254.

Bishop RF, Hill R and Mott NF. (1945). The theory of indention and hardness tests, *Proc. Phys. Soc.*, 57, 147-159.

Booker JR and Davis EH. (1972). General Treatment of Plastic Anisotropy Under Conditions of Plane Strain. *Jrnl. of Mechanics of Physics of Solids*, Vol 20, 239-250.

Brinch Hansen J. (1970). *Bulletin 28: A Revised And Extended Formula For Bearing Capacity*, Copenhagen, Danish Geotechnical Institute.

Bransby MF and Randolph MF. (1998). Combined loading of skirted foundations. *Geotechnique*; 48(5): 637-655.

Brown JD and Meyerhof GG. (1969). Experimental study of bearing capacity in layered clays. *Proc. Seventh Intl. Conf. Soil Mech. Found. Engrg.*, Mexico City,Vol. 2, 45-51.

Calladine CR. (1969). *Engineering Plasticity*, Pergamon Press. 318pp.

Chen WF. (1975). *Limit Analysis and Soil Plasticity*, Elsevier Publishing Co., Amsterdam. 638pp.

Chen WF and Liu XL. (1990). *Limit Analysis in Soil Mechanics*, Elsevier Publishing Co., Amsterdam. 477pp.

Chen WF and McCarron WO. (1991). Bearing Capacity of Shallow Foundations. *Chapter 4, Foundation Engineering Handbook*, 2nd Edition, 144-165.

Cox AD, Eason G and Hopkins HG. (1961). Axially Symmetric plastic deformation in soils, *Phil. Trans. Royal Society of London*, Series A, 254, 1-45.

Davis EH. (1968). Theories of Plasticity and the Failure of Soil Masses. *Soil Mechanics: Selected Topics*, ed. IK Lee, 341-380.

Davis EH and Booker JR. (1973). "The effect of increasing strength with depth on the bearing capacity of clays", *Geotechnique*, 23(4), 551-563.

Drucker DC. 1953. Limit Analysis of Two and Three Dimensional Soil Mechanics Problems. *Jrnl. of the Mechanics and Physics of Solids.* Vol. 1, 217-226.

Drucker DC and Prager W. (1952). Soil Mechanics and Plastic Analysis or Limit Design, *Qrtly. Of Applied Mathematics*, Vol. X, No. 2, 157-165.

Gourvenec S and Randolph MF. (2003). Effect of strength non-homogeniety on the shape of failure envelopes for combined loading of strip and circular foundations on clay. Geotechnique, 53(6), 575-586.

Green AP. (1954). The plastic yielding of metal junctions due to combined shear and pressure. *J. Mech. Phys. Solids* 2(3): 197-211.

Hanna AM and Meyerhof GG. (1980). Design charts for ultimate bearing capacity of foundations on sand overlying soft clay. *Canadian Geotech. Jrnl*., 17, 300-303.

Heyman J. (1973). Simple Plastic Theory Applied to Soil Mechanics, *Proc. of the Symp. on Plasticity and Soil Mechanics*, Cambridge. 161-172.

Houlsby GT and Puzrin AM. (1999). The bearing capacity of a strip footing on clay under combined loading. *Proc. R. Soc. Lond.* A 455: 893-916.

Jeanjean P, Watson PG, Kolk HJ and Lacasse S. (2010). RP2GEO:The new API Recommended Practice for Geotechnical Engineering, *Proc. Offshore Tech. Conf.* OTC 20631, 1-38.

Meyerhof GG. (1951). The Ultimate Bearing Capacity of Foundations, *Geotechnique*, Vol. 2, 301-332.

Meyerhof GG. (1953). The bearing capacity of footings under eccentric and inclined loads, *Proc. Third Int. Conf. Soil Mech. And Found. Engrg.* 440-445.

Matlock H. (1970). Correlations for Design of Laterally Loaded Piles in Soft Clay, *Proc. Offshore Tech. Conf.*, OTC1204. Houston, pp. 577-594.

Murff JD. (1978). Upper Bound Analysis of Incompressible, Anisotropic Media, *Proceedings of the Society of Engineering Science*, 15th Annual Meeting, Gainesville, 521-526.

Murff JD. (1987). Plastic collapse of long piles under inclined loading, *Int. J. Numerical and Analytical Methods in Geomechanics*, 11, 185-192.

Murff JD. (1994). Limit analysis of multi-footing foundation systems, *Proc. Eighth Int. Conf. On Computer Methods and Advances in Geomechanics*, 233-244.

Murff JD. (1999). The Mechanics of Pile Foundation Collapse, ASCE Special Technical Publication, *Analysis, Design, Construction, and testing of Deep Foundations*, Proceedings of the 1999 OTRC '99 Conference, Ed. JM Roessett, 76-95.

Murff JD and Hamilton JM. (1993). P-Ultimate for undrained analysis of laterally loaded piles. *ASCE Journal of Geotechnical Engineering*. 119 (1): 91-107.

Murff JD and Miller TW. (1977a). "Foundation Stability on Non-Homogeneous Clays", *J. of the Geotechnical Engineering Division*, ASCE, 103(GT10), 1083-1095.

Murff JD and Miller TW. (1977b). "Stability Of Offshore Gravity Structure Foundations Using The Upper Bound Method", *Proc. Offshore Tech. Conf.*, Houston, 147-154.

Murff JD and Miller TW. (1980). " Shallow Penetration of Marine Foundations", ASCE *Proceedings of the Symposium on Limit Equilibrium, Plasticity, and Generalized Stress-Strain Applications in Geotechnical Engineering*, ASCE Annual Convention, Hollywood Florida, 139-152.

Murff JD and Wesselink BD. (1986). "Collapse Analysis of Pile Foundations", *Proc. Third Int. Conf. On Numerical Methods in Offshore Piling*, Nantes, 445-459.

Olsen RE and Dennis ND. (1982). *Review and Compilation of Pile Test Results, Axial Pile Capacity*, Final Report to American Petroleum Institute on Project PRAC 81-29, Univ. Texas at Austin.

Pelletier JH, Murff JD and Young AG. (1993) Historical Development and Assessment of the Current API Design Methods for Axially Loaded Piles. *Proc. Offshore Tech. Conf.*, OTC7157, Houston, 253-282.

Prager W. (1959. A*n Introduction to the Theory Of Plasticity*. Reading, Mass., Addison Wesley, 148pp.

Prandtl L. (1921). Eindringungsfestigkeit und festigkeit von schneiden, *Zeit. f. Angew. Math. u. Mech.*, 1, 15.

Pratt JA, Priest T and Casteneda CJ. (1997), *Offshore Pioneers*, Houston, Gulf Publishing Co., 302pp.

Randolph MF. Personal Communication.

Randolph MF and Houlsby GT. (1984). The limiting pressure on a circular pile loaded laterally in cohesive soil, *Geotechnique* 34(4), 613-623.

Randolph MF and Murphy BS. (1985). Shaft Capacity of Driven Piles in Clay, *Proc. Offshore Tech. Conf.*, OTC 4883. Houston, 1-8.

Reissner H. (1924), Zum Erddruckproblem, *Proc. First Int. Conf. on Applied Mechanics*, Delft, 295-311.

Sokolovskii VV. (1965). *Statics of Granular Media*, New York, Pergamon Press. 270pp.

Teng WC. (1962). *Foundation Design*. Englewood Cliffs, NJ, Prentice Hall, 466pp.

Terzaghi K. (1943). *Theoretical Soil Mechanics*. New York. J. Wiley and Son. 528pp.

Vesic AS. (1975). "Bearing Capacity Of Shallow Foundations", *Foundation Engineering Handbook*, HF Winterkorn and HY Fang (Eds), New York, van Nostrand Reinhold, 121-147.

9. Appendices

Appendix I. Upper Bound Calculations for Energy Dissipation Rates for the Brinch Hansen Mechanism

This Appendix provides examples of detailed upper bound calculations of energy dissipation rates for the Brinch Hansen failure mechanism shown in Figure 15 including variable soil strength with depth. These examples will only describe the right side of the mechanism for $x_o < 0$. With slight modifications in the values of R_1 and R_2 the calculations for the other components follow the same pattern. A general description of the mechanism is provided in the main text.

The rigid sector EFI slips along the arc EF due to the virtual rotation rate, $\dot{\beta}$, about the center of rotation O at x_o, y_o. The energy dissipation rate (hereafter called EDR) for a uniform strength soil is then

$$\dot{D}_{EF} = v_{EF} * s_u * l_{EF} = R_1\dot{\beta} * s_u * R_1\theta_2 = {y_o}^2\left[\tan^{-1}\left(\frac{x_o + B}{y_o}\right)\right] s_u\dot{\beta} \qquad \text{(I-1)}$$

Now, to generalize the result for a variable shear strength with depth we must express s_u as a function

of local coordinates and integrate along EF as follows,

$$\dot{D}_{EF} = \int_0^{\tan^{-1}\frac{x_o+B}{y_o}} y_o\dot{\beta} * s_u(y) * y_o d\theta \quad \text{(I-2)}$$

For simple strength variations, the integration can be done analytically but for general variations numerical integration may be required. Note that for a linearly increasing strength profile, common in offshore applications, s_u is as follows

$$s_u = s_{uo} + ky = s_{uo} + k[y_o(1-\cos\theta)] \quad \text{(I-3)}$$

To calculate the EDR along FG we use a local coordinate system centered at I as shown in Figure 15. Again the general case requires integration as follows,

$$\dot{D}_{FG} = \int_{\frac{\pi}{4}}^{\frac{\pi}{2}+\tan^{-1}\left(\frac{x_o+B}{y_o}\right)} R_1\dot{\beta}s_u(y) * (R_2-R_1)d\theta \quad \text{(I-4)}$$

where

$$R_2 = \sqrt{(x_o+B)^2 + {y_o}^2} \quad \text{(I-5)}$$

and the depth from the soil surface in local coordinates is

$$y = (R_2 - R_1)\sin\theta \quad \text{(I-6)}$$

The EDR in the sector FGI is calculated using the same local coordinate system as for FG. In this radial shear fan however the tangential velocity varies linearly along the radius, r, as follows

$$v_\theta = (R_2 - r)\dot{\beta} \quad \text{(I-7)}$$

The only non-zero strain increment term is then

$$\dot{\varepsilon}_{r\theta} = \frac{1}{2}\left(\frac{\partial v_r}{r\partial\theta} + \frac{\partial v_\theta}{\partial r} - \frac{v_\theta}{r}\right) = \frac{-R_2\dot{\beta}}{2r} \quad \text{(I-8)}$$

The maximum principal strain increment is then

$$|\dot{\varepsilon}|_{max} = \frac{R_2\dot{\beta}}{2r} \quad \text{(I-9)}$$

And the EDR is then

$$\dot{D}_{FGI} = \int_0^{R_2-R_1}\int_{\frac{\pi}{4}}^{\frac{\pi}{2}+\tan^{-1}\left(\frac{x_o+B}{y_o}\right)} \frac{R_2\dot{\beta}}{r} * s_u(y) * r d\theta dr \quad \text{(I-10)}$$

where

$$y = r\sin\theta \quad \text{(I-11)}$$

The velocity along GH is also equal to $R_1\dot{\beta}$ so the EDR is integrated along GH. The local coordinate system for this calculation is a rectangular system with origin at G and the x' axis along GH. The EDR is then

$$\dot{D}_{GH} = \int_0^{R_2-R_1} R_1\dot{\beta} * s_u(y) * dx' \quad \text{(I-12)}$$

The depth *y* in local coordinates is then

$$y = \frac{R_2 - R_1 - x'}{\sqrt{2}} \quad \text{(I-13)}$$

The triangular region GHI is deforming to conform to the varying velocity along GI. Using the same coordinate system as for GH, the only non-zero velocity is

$$v_{x'} = (R_1 + y')\dot{\beta} \quad \text{(I-14)}$$

Thus the only non-zero strain increment component is then

$$\dot{\varepsilon}_{x'y'} = \frac{1}{2}\left(\frac{\partial v_{x'}}{\partial y'} + \frac{\partial v_{y'}}{\partial x'}\right) = \frac{1}{2}\dot{\beta} \quad \text{(I-15)}$$

Since the strain increment is a constant, we can carry out the integration in yet a simpler coordinate system with origin at G and the x'' axis parallel to the soil surface. The EDR is then

$$\dot{D}_{GHI} = 2\int_0^{\frac{R_2-R_1}{\sqrt{2}}} y'' * s_u(y) * dy'' \quad \text{(I-16)}$$

where

$$y = \frac{R_2 - R_1}{\sqrt{2}} - y'' \quad \text{(I-17)}$$

As mentioned above the calculations for the remaining components follow in a similar manner.

Appendix II. Upper Bound Calculations for Energy Dissipation Rates for the Squeeze Mechanism

This Appendix provides examples of detailed upper bound calculations of energy dissipation rates for the squeeze failure mechanism shown in Figure 19. The EDRs are determined within the continuous thin layer ABCD, at the interfaces AD and BC, along the slope CE and at the thin layer-wedge interface CD. The mechanism is symmetric so only the right hand side is detailed below.

In region ABCD it is assumed that the vertical velocity is given as

$$v_y = v_o\left(1 - \frac{y}{t}\right) \tag{II-1}$$

Where $t =$ thin layer thickness. Since the deformation field is incompressible we can say that

$$\dot{\varepsilon}_v = \dot{\varepsilon}_x + \dot{\varepsilon}_y = 0 \;\Rightarrow\; \dot{\varepsilon}_x = \frac{v_o}{t} \tag{II-2}$$

The EDR within region ABCD is then

$$\dot{D}_{ABCD} = \frac{2s_u v_o}{t} \tag{II-3}$$

Since the EDR is constant throughout ABCD the total EDR is then simply $= s_u B$.

It can be shown that v_x in region ABCD is a function of x only by integrating Equation II-2 to get

$$v_x = \frac{v_o}{t}x + f(y) \tag{II-4}$$

Since $v_x = 0$ at $x = 0$ the function, $f(y)$, in Equation II-4 is zero. Assuming the interface strength at BC is s_u, the dissipation along BC is

$$\dot{D}_{BC} = s_u v_o \int_0^{B/2} \frac{v_o}{t} x dx = \frac{s_u v_o B^2}{8t} \tag{II-5}$$

If we assume full adhesion of the soil along AD, the EDR is equal to that along BC or for no adhesion the EDR along AD is zero.

From Equation II-4, the velocity v_x along CD is equal to $v_o B/2t$. The wedge CED then remains rigid and the EDR along CE is

$$\dot{D}_{CE} = \frac{v_o B}{2t\cos\theta} * \frac{t}{\sin\theta} * s_u = \frac{v_o B s_u}{2\sin\theta\cos\theta} \tag{II-6}$$

At the interface CD the vertical velocity of the squeezing zone is downward (Equation II-1) and the vertical velocity of the wedge is upward given by

$$v_y = -\frac{v_o B\tan\theta}{2t} \tag{II-7}$$

Because the velocities are in opposite directions the relative velocity is the relevant value to calculate the dissipation. This is a function of *y* and is therefore integrated along CD to give

$$\dot{D}_{CD} = v_o s_u\left(\frac{B\tan\theta}{2} + \frac{t}{2}\right) \tag{II-8}$$

The *EDR* terms determined here are summed, multiplied by two (for symmetry) and set equal to the external work rate, Vv_o. The resulting vertical load V, given in Equation 37 in the main text is then minimized with respect to θ to give the best upper bound.